# SERGHEI (-SWE) v1.0: a performance portable HPC shallow water solver for hydrology and environmental hydraulics

Daniel Caviedes-Voullième[1,2], Mario Morales-Hernández[3,4], Matthew R. Norman[4], and
Ilhan Özgen-Xian[5,6]

[1]Simulation and Data Lab Terrestrial Systems, Jülich Supercomputing Centre, Forschungszentrum Jülich (Germany)
[2]Institute of Bio- and Geosciences: Agrosphere (IBG-3), Forschungszentrum Jülich (Germany)
[3]Fluid Mechanics, I3A-Universidad de Zaragoza (Spain)
[4]Oak Ridge National Laboratory (USA)
[5]Institute of Geoecology, Technische Universität Braunschweig (Germany)
[6]Earth & Environmental Sciences Area, Lawrence Berkeley National Laboratory (USA)

**Correspondence:** Daniel Caviedes-Voullième (d.cavides.voullieme@fz-juelich.de)

**Abstract.** The Simulation EnviRonment for Geomorphology, Hydrodynamics and Ecohydrology in Integrated form (SERGHEI) is a multi-dimensional, multi-domain and multi-physics model framework for environmental and landscape simulation, designed with an outlook towards Earth System Modelling. At the core of SERGHEI's innovation is its performance-portable HPC implementation, built from scratch on the Kokkos portability layer, allowing to deploy SERGHEI, in a performance-portable fashion, in GPU-based heterogeneous systems. In this work we explore combinations of MPI and Kokkos using OpenMP and CUDA backends. In this contribution, we introduce the SERGHEI model framework, and present with detail its first operational module for solving shallow water equations (SERGHEI-SWE) and its HPC implementation. This module is designed to be applicable to hydrological and environmental problems including flooding and runoff generation, with an outlook towards Earth System Modelling. Its applicability is demonstrated by testing several well-known benchmarks and large scale problems for which SERGHEI-SWE achieves excellent results for the different types of shallow water problems. Finally, SERGHEI-SWE scalability and performance-portability is demonstrated and evaluated on on several TOP500 HPC systems, with very good scaling in the range of over 20000 CPUs and up to 256 state-of-the art GPUs.

## 1 Introduction

The upcoming exascale high-performance parallel computing (HPC) systems will enable physics-based geoscientific modelling with unprecedented detail (Alexander et al., 2020). Although the need for such HPC systems is traditionally driven by climate, ocean, and atmospheric modelling, hydrological models are progressively becoming as physical, sophisticated, and computationally intensive. Physically-based, integrated hydrological models such as Parflow (Kuffour et al., 2020), Amanzi/ATS (Coon et al., 2019), and Hydrogeosphere (Brunner and Simmons, 2012) are becoming more prominent in hydrological

20  research and Earth System Modelling (ESM) (Fatichi et al., 2016; Paniconi and Putti, 2015), making HPC more and more relevant for computational hydrology (Clark et al., 2017).

Hydrological models, as many other HPC applications, are currently facing challenges in exploiting available and future HPC systems. These challenges arise, not only because of the intrinsic complexity of maintaining complex codes over large periods of time, but because HPC and its hardware are undergoing a large paradigm change (Leiserson et al., 2020; Mann, 25  2020), which is strongly driven by the end of Moore's law (Morales-Hernández et al., 2020). In order to gain higher processing capacity, computers will require heterogeneous and specialised hardware (Leiserson et al., 2020), potentially making high-performing code harder to develop and maintain, and demanding for developers to adapt and optimise code for an evolving hardware landscape. It has become clear that upcoming exascale systems will have heterogeneous architectures embedded in modular and reconfigurable architectures (Djemame and Carr, 2020; Suarez et al., 2019) that will consist of different types of 30  CPUs and accelerators, possibly from multiple vendors requiring different programming models. This puts pressure on domain scientists to write *portable* code that *performs* efficiently on a range of existing and future HPC architectures (Bauer et al., 2021; Lawrence et al., 2018; Schulthess, 2015), and to ensure the *sustainability* of such code (Gan et al., 2020).

Different strategies are currently being developed to cope with this grand challenge. One strategy is to offload the architecture-dependent parallelisation tasks to the compiler—see, for example, (Vanderbauwhede and Takemi, 2013; Vanderbauwhede and 35  Davidson, 2018; Vanderbauwhede, 2021). Another strategy is to use an abstraction layer that provides a unified programming interface to different computational backends—a so-called *performance portability framework*—that allows the same code to be compiled across different HPC architectures. Examples of this strategy include RAJA (Beckingsale et al., 2019) and Kokkos (Edwards et al., 2014; Trott et al., 2021), which are both very similar in their scope and their capability. Both RAJA and Kokkos are C++ libraries that implement a shared-memory programming model to maximise the amount of code that 40  can be compiled across different hardware devices with nearly the same parallel performance. They allow access to several computational backends, in particular multi-GPU and heterogeneous HPC systems.

This paper introduces the Kokkos-based computational (eco)hydrology framework SERGHEI (Simulation EnviRonment for Geomorphology, Hydrodynamics and Ecohydrology in Integrated form) and its surface hydrology module SERGHEI-SWE. The primary aim of SERGHEI's implementation is scalability and performance-portability. In order to achieve this, 45  SERGHEI is written in C++ and based from scratch on the Kokkos abstraction. Kokkos currently supports CUDA, OpenMP, HIP, SYCL, and Pthreads as backends. We chose Kokkos over other alternatives, because it is actively engaged in securing the sustainability of its programming model, fostering its partial inclusion into ISO C++ standards (Trott et al., 2021). Indeed, there is an increasing number of applications in multiple domains leveraging on Kokkos, for example (Bertagna et al., 2019; Demeshko et al., 2018; Grete et al., 2021; Halver et al., 2020; Watkins et al., 2020). Thus, among other similar solutions, 50  Kokkos has been identified as advantageous in terms of performance portability and project sustainability, although perhaps somewhat more invasive and less clear on the resulting code (Artigues et al., 2019). We present the full implementation of the SERGHEI-SWE module, the shallow water equations (SWE) solver for free surface hydrodynamics at the heart of SERGHEI.

SERGHEI-SWE enables the simulation of surface hydrodynamics of overland and stream flow seamlessly and across scales. Historically, hydrological models featuring surface flow have relied on kinematic or zero-inertia (diffusive) approximations

due to their apparent simplicity (Caviedes-Voullième et al., 2018; Kollet et al., 2017) and because until the last decade, robust SWE solvers were not available (Caviedes-Voullième et al., 2020a; García-Navarro et al., 2019; Simons et al., 2014; Özgen-Xian et al., 2021). However, the current capabilities of SWE solvers, the increase in computational capabilities, and the need to better exploit parallelism—easier to achieve with explicit solvers than implicit solvers as usually required by diffusive equations (Caviedes-Voullième et al., 2018; Fernández-Pato and García-Navarro, 2016)—has been pushing to replace simplified surface flow models (for hydrological purposes) with fully dynamic SWE solvers. There is an increasing number of studies using SWE solvers for rainfall-runoff and overland flow simulations from hillslope to catchment scales—for example, (Bellos and Tsakiris, 2016; Bout and Jetten, 2018; Caviedes-Voullième et al., 2012, 2020a; Costabile and Costanzo, 2021; Costabile et al., 2021; David and Schmalz, 2021; Dullo et al., 2021a, b; Fernández-Pato et al., 2020; García-Alén et al., 2022; Simons et al., 2014; Xia and Liang, 2018). This trend contributes to the transition from engineering hydrology towards Earth System science (Sivapalan, 2018), a shift that motivated by necessity and opportunity, as continental (and larger) ESM will progressively require fully dynamic SWE solvers to cope with increased resolution digital terrain models and the dynamics which respond to them, improved spatiotemporal rainfall data and simulations, as well as increasingly more sophisticated process interactions across scales, from patch, to hillslope to catchments (Fan et al., 2019).

SERGHEI-SWE distinguishes itself from other HPC SWE solvers through a number of key novelties. Firstly, SERGHEI-SWE is open sourced under a permissive BSD license. While there are indeed many GPU-enabled SWE codes, many of these are research codes that are not openly available—for example, (Aureli et al., 2020; Buttinger-Kreuzhuber et al., 2022; Echeverribar et al., 2020; Hou et al., 2020; Lacasta et al., 2014, 2015; Liang et al., 2016; Vacondio et al., 2017)—or commercial codes, such as RiverFlow2D, TUFLOW, HydroAS_2D—see Jodhani et al. (2021) for a recent non-comprehensive review. Open source solvers are a fundamental need for the community, ensuring transparency, reproducibility, and providing a base for model (software) sustainability. We note that open source SWE solvers are becoming increasingly more available—see Table 1. However, only a handful of these freely available models are enabled for GPUs, mostly through CUDA. Fewer of them have multi-GPU capabilities and are capable of fully leveraging HPC hardware. All of these multi-GPU enabled codes are currently dependent on CUDA, and therefore somewhat limited to Nvidia hardware. This leads into the second and most relevant novelty of SERGHEI-SWE: it is a performance-portable, highly scalable and GPU enabled solver. SERGHEI-SWE generalises hardware (CPU, GPU, accelerators) support to a performance-portability concept through Kokkos. This gives SERGHEI-SWE the key advantage to have a single code base for the currently fully operational OpenMP and CUDA backends, as well as HIP, currently experimental in SERGHEI, but most importantly, keeps this code base relevant for other backends, such as SYCL. This is particularly important, as the current HPC landscape features not only Nvidia GPUs, but a currently increased adoption of AMD GPUs, with the most recent leading TOP 500 systems –Frontier and LUMI–, as well as upcoming systems (e.g., El Capitan) relying on AMD GPUs. In this way, SERGHEI is safely avoiding the vendor lock trap.

SERGHEI-SWE has been developed harnessing the past 15 years of numerical advances in the solution of SWE, ranging from fundamental numerical formulations (Echeverribar et al., 2019; Morales-Hernández et al., 2020) to HPC GPU implementations (Brodtkorb et al., 2012; Hou et al., 2020; Lacasta et al., 2014, 2015; Liang et al., 2016; Vacondio et al., 2017; Sharif et al., 2020). Most of this work was done in the context of developing solvers for flood modelling, with rather engi-

| Model | Reference | GPU | MPI | Availability | Notes |
|---|---|---|---|---|---|
| SERGHEI-SWE | this paper | Kokkos | yes | Open source (BSD) | Highly scalable |
| TRITON | Morales-Hernández et al. (2021) | CUDA | yes | Open source (BSD) | Highly scalable |
| PARFLOOD | Vacondio et al. (2014) | CUDA | yes | - | Highly scalable, source code can be requested, MPI parallelisation by Turchetto et al. (2019) |
| HiPIMS | Xia et al. (2019) | CUDA | - | Open source (GPLv3) | Multi-GPU support based on Thrust (on single node) |
| DRR/FI | Kobayashi et al. (2015) | - | yes | - | Highly scalable |
| SW2D-GPU | Carlotto et al. (2021) | CUDA | - | Open source | - |
| LisFlood-FP 8.0 | Shaw et al. (2020) | CUDA | - | Open source (BSD) | SWE solver embedded into LisFlood (Bates and Roo, 2000), which originally did not solve SWE. |
| IBER | García-Feal et al. (2018) | CUDA | - | Freeware | - |
| SW2D-Lemon | Caldas Steinstraesser et al. (2021) | - | - | Freeware | Source code can be requested |
| B-flood | Kirstetter et al. (2021) | - | - | Open source (GPL) | Adaptive mesh refinement |
| FullSWOF | Delestre et al. (2017) | - | yes | Open source (CeCILL) | MPI parallelisation by (Wittmann et al., 2017) |
| TELEMAC | Moulinec et al. (2011) | - | yes | Open source (GPLv3/LGPL) | - |
| GeoClaw | Berger et al. (2011) | - | yes | Open source (BSD) | Adaptive mesh refinement |
| HEC-RAS2D | Brunner (2021) | - | - | Freeware | - |
| hms | Simons et al. (2014) | - | yes | Open source (GPL) | MPI parallelisation by Steffen et al. (2020) |

**Table 1.** Overview of openly available SWE solvers.

90  neering oriented applications, demanding high quantitative accuracy and predictive capability. Most of the established models in Table 1 were developed within such context, although many are currently also adopted for more hydrological applications. Leveraging on this technology, SERGHEI-SWE is designed to cope with the classical shallow water applications of fluvial and urban flooding, as well as the emerging rainfall-runoff problems in both natural and urban environments (for which coupling to sewer system models is a longer term objective), as well as other flows of broad hydrological and environmental interest that

95  occur on (eco)hydrological time scales, priming it for further uses in ecohydrology and geomorphology. Nevertheless, all shallow water applications should benefit from the high performance and high scalability of SERGHEI-SWE. With an HPC-ready SWE solver, catchment scale rainfall-runoff applications around the $1\,\mathrm{m}^2$ resolution are feasible. Similarly, large river and floodplain simulations can be enabled for operational flood forecasting, and flash floods in urban environments can be tackled with extremely high spatial resolution. Moreover, it is noteworthy that SERGHEI-SWE is not confined to HPC environments,

100  and users with workstations can also benefit from improved performance.

## 1.1 The SERGHEI framework

SERGHEI is envisioned as a modular simulation framework around a physically-based hydrodynamic core, which allows to represent a variety of water-driven and water-limited processes in a flexible manner. In this sense, SERGHEI is based on the idea of water fluxes as a connecting thread among various components and processes within the Earth system (Giardino

105  and Houser, 2015). As illustrated by the conceptual framework in Figure 1, SERGHEI's hydrodynamic core will consist of mechanistic surface (SERGHEI-SWE, the focus of this paper) and subsurface flow solvers (light and dark blue), around which a generalised transport framework for multi-species transport and reaction will be implemented (gray). The transport framework will further enable the implementation of morphodynamics (gold) and vegetation dynamics (green) models. The transport
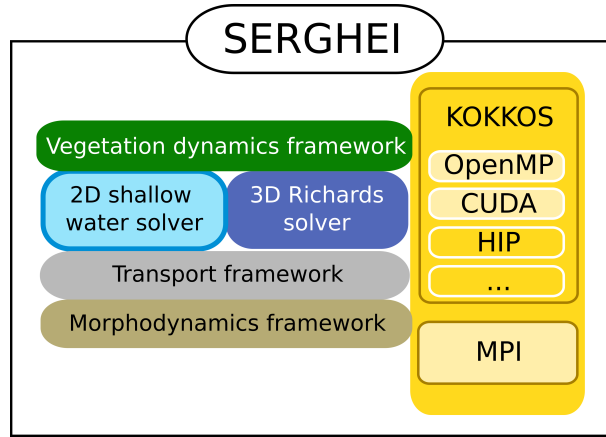
**Figure 1.** A conceptual framework of SERGHEI

framework will also include a Lagrangian particle-tracking module (currently also under development). At the time of the writing of this paper, the subsurface flow solver—based on the three-dimensional extension of the Richards solver by Li et al. (2021)—is experimentally operative and is underway to be coupled to the surface flow solver, thus, making the hydrodynamic core of SERGHEI applicable to integrated surface–subsurface hydrology. The initial infrastructure for the transport-based three other frameworks is currently under development.

## 2  Mathematical and numerical model of SERGHEI-SWE

In this section we provide an overview of the underlying mathematical model and the numerical schemes implemented in SERGHEI-SWE. The implementation is based on well-established numerical schemes, and consequently, we limit this to a minimal presentation.

SERGHEI-SWE is based on the resolution of the two-dimensional (2D) shallow water equations, that can be expressed in a compact differential conservative form as:

$$
\left.
\begin{aligned}
&\frac{\partial \mathbf{U}}{\partial t} + \frac{\partial \mathbf{F}}{\partial x} + \frac{\partial \mathbf{G}}{\partial y} = \mathbf{S_r} + \mathbf{S_b} + \mathbf{S_f}, \\[2mm]
&\mathbf{U} = \begin{bmatrix} h \\ q_x \\ q_y \end{bmatrix} \quad
\mathbf{F} = \begin{bmatrix} q_x \\ \dfrac{q_x^2}{h} + \dfrac{1}{2}gh^2 \\ \dfrac{q_x q_y}{h} \end{bmatrix} \quad
\mathbf{G} = \begin{bmatrix} q_y \\ \dfrac{q_x q_y}{h} \\ \dfrac{q_y^2}{h} + \dfrac{1}{2}gh^2 \end{bmatrix}, \\[2mm]
&\mathbf{S_r} = \begin{bmatrix} r_o - r_f \\ 0 \\ 0 \end{bmatrix} \quad
\mathbf{S_b} = \begin{bmatrix} 0 \\ -gh\dfrac{\partial z}{\partial x} \\ -gh\dfrac{\partial z}{\partial y} \end{bmatrix} \quad
\mathbf{S_f} = \begin{bmatrix} 0 \\ -\sigma_x \\ -\sigma_y \end{bmatrix}.
\end{aligned}
\right\}
\tag{1}
$$

Here, $t$ [T] is time, $x$ [L] and $y$ [L] are Cartesian coordinates, $\mathbf{U}$ is the vector of conserved variables (that is to say the unknowns of the system) containing the water depth, $h$ [L], and the unit discharges in $x$ and $y$ directions, called $q_x = hu$ [L$^2$T$^{-1}$] and $q_y = hv$ [L$^2$T$^{-1}$] respectively. $\mathbf{F}$ and $\mathbf{G}$ are the fluxes of these conserved variables with gravitational acceleration $g$ [LT$^{-2}$]. The mass source terms $\mathbf{S}_r$ account for rainfall, $r_o$ [LT$^{-1}$], and infiltration/exfiltration, $r_f$ [LT$^{-1}$]. The momentum source terms include gravitational bed slope terms, $\mathbf{S_b}$, expressed according to the gradient of the elevation $z$ [L]; and friction terms, $\mathbf{S_f}$, as a function of the friction slope $\sigma$. This friction slope is often modelled by means of Gauckler-Manning's equation in terms of Manning's roughness coefficient $n$ [TL$^{-1/3}$], but also frequently with the Chezy and the Darcy-Weisbach formulations (Caviedes-Voullième et al., 2020a). In addition, specialised formulations of the friction slope exist to consider the effect of microtopography and vegetation for small water depths, e.g., variable Manning's coefficients (Jain and Kothyari, 2004; Mügler et al., 2011) or generalised friction laws (Özgen et al., 2015b). A recent systematic comparison and in-depth discussion of several friction models with a focus on rainfall-runoff simulations is given in Crompton et al. (2020). Implementing additional friction models is of course possible, and relevant, especially to address the multiscale nature of runoff in catchments, but not essential to the points in this paper. The observant reader will note that in Equation 1, viscous and turbulent fluxes have been neglected. The focus here is on applications (rainfall-runoff, dam-breaks) where the influence of these can be safely neglected. Turbulent viscosity may become significant for ecohydraulic simulations of river flow, and turbulent fluxes play of course an important role in mixing in transport simulations. We will address these issues in future implementations of the transport solvers in SERGHEI.

SERGHEI-SWE uses a first-order accurate upwind finite-volume scheme with a forward Euler time integration to solve the system of equations (1) on uniform Cartesian grids with grid spacing $\Delta x$ [L]. The numerical scheme, presented in detail in (Morales-Hernández et al., 2021), harnesses many solutions that have been reported in the literature in the past decade, ensuring that all desirable properties of the scheme (well-balancing, depth-positivity, stability, robustness) are preserved under the complex conditions of realistic environmental problems. In particular, we require the numerical scheme to stay robust and accurate in the presence of arbitrary rough topography and shallow water depths with wetting and drying.

Well-balancing and water depth positivity are ensured by solving numerical fluxes at each cell edge $k$ with augmented Riemann solvers (Murillo and García-Navarro, 2010, 2012) based on the Roe linearisation (Roe, 1981). In fluctuation form, the rule for updating the conserved variables in cell $i$ from time step $n$ to time step $n+1$ reads:

$$\mathbf{U}_i^{\star} = \mathbf{U}_i^n - \frac{\Delta t}{\Delta x} \sum_{k=1}^{4} \sum_{m=1}^{3} \frac{\tilde{\lambda}^-}{\tilde{\lambda}} \left[ (\tilde{\lambda}\tilde{\alpha} - \tilde{\beta})\tilde{\mathbf{e}} \right]_{m,k}^n, \tag{2}$$

followed by

$$\mathbf{U}_i^{n+1} = \mathbf{U}_i^{\star} + (r_o - r_f)_i^n \Delta t, \tag{3}$$

where $\tilde{\lambda}$ and $\tilde{\mathbf{e}}$ are the eigenvalues and eigenvectors of the linearised system of equations, $\tilde{\alpha}$ and $\tilde{\beta}$ are the fluxes and bed slope and friction source term linearisations respectively, and the minus-sign accounts for the upwind discretisation. Note that all the *tilde* variables are defined at each computational edge. The time step $\Delta t$ is restricted to ensure stability, following the Courant-Friedrich-Lewy (CFL) condition:

$$\Delta t = \text{CFL} \min_i \left\{ \frac{\Delta x}{\left| \frac{q_x}{h} \right|_i + \sqrt{gh_i}, \left| \frac{q_y}{h} \right|_i + \sqrt{gh_i}} \right\} \qquad \text{CFL} \leq 0.5 \tag{4}$$

Although the wave speed values are formally defined at the interfaces, the corresponding cell values are used instead for the CFL condition. As pointed in (Morales-Hernández et al., 2021), this approach does not compromise the stability of the system, but accelerates the computations and simplifies the implementation.

It is relevant to acknowledge that second (and higher) order schemes for SWE are available (e.g. Buttinger-Kreuzhuber et al., 2019; Caviedes-Voullième et al., 2020b; Hou et al., 2015; Navas-Montilla and Murillo, 2018). However, first order schemes are still a pragmatic choice (Ayog et al., 2021), especially when dealing with very high resolution (as targeted with SERGHEI) which offsets their higher discretisation error and numerical diffusivity in comparison to higher order schemes. Similarly, robust schemes for unstructured triangular meshes are well established, together with their well-known advantages in reducing cell counts and numerical diffusion (Bomers et al., 2019; Caviedes-Voullième et al., 2012, 2020a). As these advantages are less relevant at very high resolution, we opt for Cartesian grids to avoid issues with memory mapping, coalescence and cache misses in GPUs (Lacasta et al., 2014) and additional memory footprint, while also making domain-decomposition simpler. Both higher order schemes and unstructured (and adaptive) meshes may be also implemented within SERGHEI.

## 3 HPC implementation of the SERGHEI framework

In this section we describe the key ingredients of the HPC implementation of SERGHEI. Conceptually, this requires, firstly, handling parallelism inside a computational device (multicore CPU or GPU) with shared memory, and the related portability and corresponding backends (i.e., OpenMP, CUDA, HIP, etc.). On a higher level of parallelism, distributing computations across many devices requires domain decomposition and a distributed memory problem, implemented via MPI. The complete implementation of SERGHEI encompasses both, distributing parallel computations into many subdomains, each of which is mapped onto a computational device. Here we start the discussion from the higher level of domain decomposition, and highlight that the novelty of SERGHEI lies with the multiple levels of parallelism, together with the performance-portable shared memory approach via Kokkos.

### 3.1 Domain decomposition

The surface domain is a two-dimensional plane, discretised by a Cartesian grid with a total cell number of $N_t = N_x N_y$, where $N_x$ and $N_y$ are the number of cells in $x$- and $y$-directions, respectively. Operations are usually performed per subdomain, each one associated with an MPI rank. During initialisation, each MPI process constructs a local subdomain with $n_x$ cells in $x$-direction and $n_y$ cells in $y$-direction. The user specifies the number of subdomains in each Cartesian direction at runtime and SERGHEI determines the subdomain size from this information. Subdomains are the same size, except for correction due to non-integer-divisible decompositions. In order to communicate information across subdomains, SERGHEI uses so-
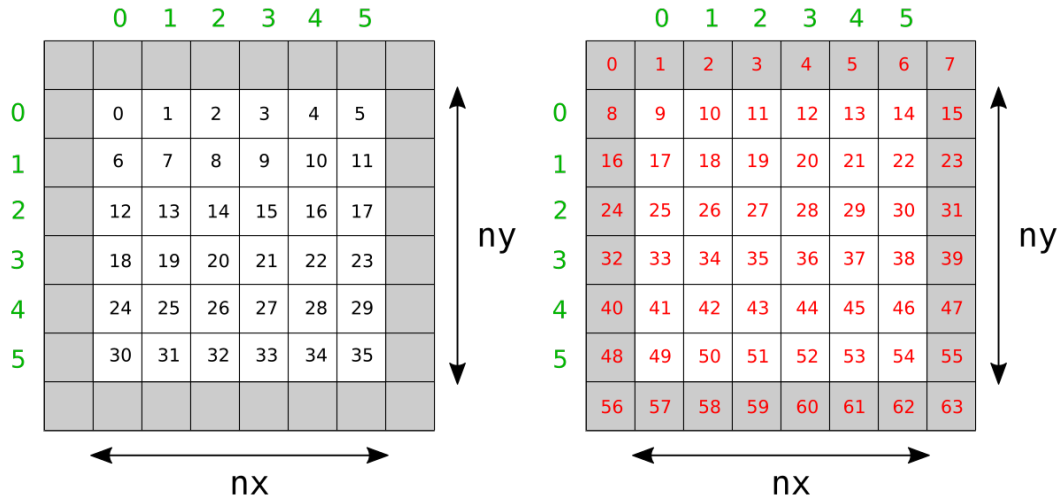
**Figure 2.** Domain decomposition and indexing in SERGHEI: A subdomain consists of physical cells (white) and halo cells (gray). SERGHEI uses two sets of indices: an index for physical cells (left) and an index for all cells including the halo cells (right)

called *halo cells*, non-physical cells on the boundaries of the subdomain that overlap with physical cells from neighbouring subdomains. The halo cells augment the number of cells in $x$- and $y$-direction by 1 at each boundary. Thus, the subdomain size
185    is $n_t = (n_x + 2)(n_y + 2)$. The definitions are sketched—without loss of generality—for a square-shaped subdomain in Figure 2 and the way these subdomains overlap in the global domain is sketched in Figure 3 (left). Halo cells are not updated as part of the time stepping. Instead, they are updated by receiving data from the neighbouring subdomain, a process which naturally requires MPI communications.

     Besides the global cell index that ranges from 0 to $N_t$, each subdomain uses two sets of local indices to access data stored
190    in its cells. The first set spans over all physical cells inside the subdomain and the second index spans over both halo cells and physical cells—see Figure 2. The second set maps into memory position. For example, in order to access the physical cell 14 in Figure 2, one has to access memory position 27.

### 3.2    Data exchange between subdomains

The underlying methods for data exchange between subdomains are centered on the subdomains rather than on the interfaces.
195    Data is exchanged through MPI-based send and receive calls (non-blocking) that aggregate data in the halo cells across the subdomains. Note that, by default, Kokkos implicitly assumes that the MPI library is GPU-aware, allowing GPU to GPU communication provided that the MPI libraries support this feature. Figure 3 (right) illustrates the concept of sending a halo buffer containing state variables from subdomain 1 to update halo cells of subdomain 0. The halo buffer contains state variables for $n_y$ cells, grouped as water depth ($h$), unit discharge in $x$-direction ($hu$), and unit discharge in $y$-direction ($hv$).
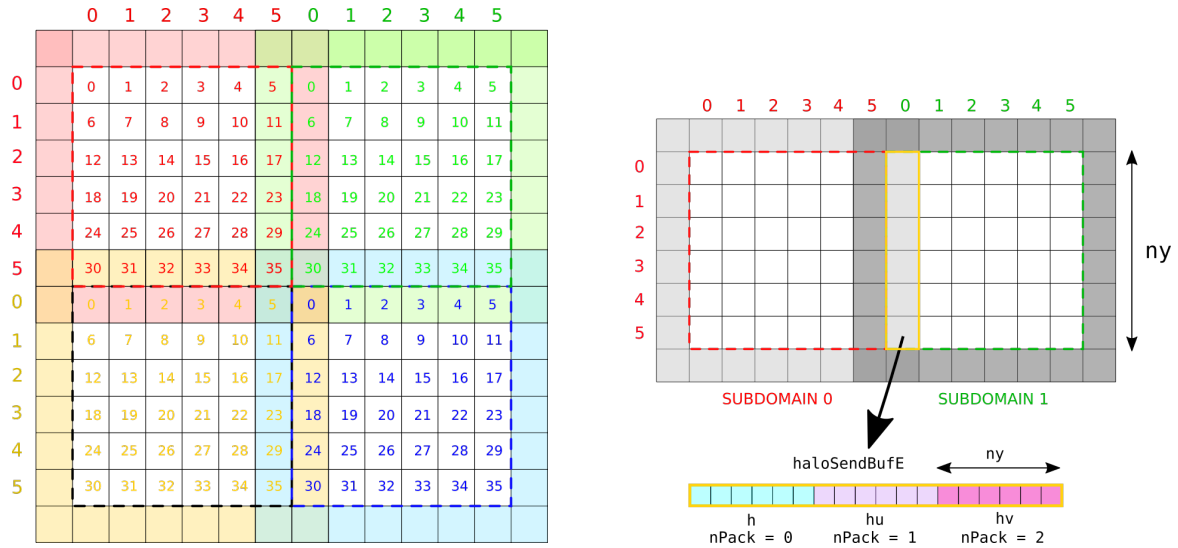
**Figure 3.** Data exchange between subdomains in SERGHEI: In the global surface domain, subdomains overlap with each other through their halo cells (left). These halo cells are used to exchange data between the subdomains (right).

## 3.3 Performance portable implementation

Intra-device parallelism is achieved per subdomain through the Kokkos framework, which allows the user to choose between shared memory parallelism and GPU backends for further acceleration. SERGHEI's implementation makes use of the Kokkos concept of `Views`, which are memory space aware abstractions. For example, for arrays of real numbers, SERGHEI defines a type `realArr`, based on `View`. This takes the form of Listing 1 for the shared (host) memory space and Listing 2 for the Unified Virtual Memory (UVM) GPU-device CUDA memory space. The UVM significantly facilitates development while avoiding writing explicit host-to-device (and viceversa) memory movements.

**Listing 1.** `realArr` definition based on View for CPU

```
typedef Kokkos::View<real*,Kokkos::LayoutRight> realArr;
```

and for a CUDA backend, making use of unified memory (`CudaUVMSpace`) is

**Listing 2.** `realArr` definition based on View for GPU

```
typedef Kokkos::View<real*,Kokkos::LayoutRight,
        Kokkos::Device<Kokkos::Cuda,Kokkos::CudaUVMSpace>> realArr;
```

Similar definitions can be constructed for integer arrays. These arrays describe spatially distributed fields, such as conserved variables, model parameters, and forcing data. Deriving these arrays from `View` allows us to operate on them via Kokkos to achieve performance portability.

Conceptually, the SERGHEI-SWE solver consists of two computationally intensive kernels: (i) cell-spanning and (ii) edge-spanning kernels. The update of the conserved variables following Equation 2 results in a kernel around a cell-spanning loop.

9

These cell-spanning loops are the most frequent ones in SERGHEI-SWE and are used for many processes, of different computational demand. The standard C++ implementation of such a kernel is illustrated in Listing 3, which spans indices `i` and `j` of a 2D cartesian grid. Here, the loops may be parallelised using, for example, OpenMP or CUDA. However, such a direct implementation of, for example an OpenMP parallelisation, would not automatically allow leveraging GPUs. That is to say, such an implementation is not portable.

**Listing 3.** Conserved variable update in standard C++

```
inline void computeNewState(State &state, const Domain &dom, const SourceSinkData &ss){
    for (int j=0; j<dom.ny; j++){
        for (int i=0; i<dom.nx; i++){
            // computationally intensive code to update cells
        }
    }
}
```

In order to achieve the desired portability, we replace the standard `for` by a `Kokkos::parallel_for`, which enables a lambda function, is minimally intrusive and reformulates this kernel to the code shown in Listing 4. As a result, this implementation can be compiled for both OpenMP applications and GPUs with Kokkos handling the low-level parallelism on different backends.

**Listing 4.** Conserved variable update using Kokkos

```
inline void computeNewState(State &state, const Domain &dom, const SourceSinkData &ss){
    Kokkos::parallel_for(dom.nCellDomain, KOKKOS_LAMBDA(int iGlob){
                    // computationally intensive code to update cells
    }
}
```

Edge-spanning loops are conceptually necessary to compute numerical fluxes (Equation 2). Although numerical fluxes can be computed in a cell-centered fashion, this would lead to inefficiencies due to duplicated computations. In Listing 5 we illustrate the edge-spanning kernel solving the numerical fluxes in SERGHEI-SWE. Notably, Listing 5 is indexed by cells, and the construction of edge-wise tuples occurs inside of the kernel. This bypasses the need for additional memory structures to hold edge-based information, but only for Cartesian meshes. Generalisation to adaptive or unstructured meshes would require explicitly an edge-based loop with an additional View of size equal to the number of edges.

**Listing 5.** Flux computations

```
inline void computeDeltaFluxXRoe(State &state, Domain const &dom,   Parallel &par) {
    Kokkos::parallel_for( dom.ncells , KOKKOS_LAMBDA (int iGlob) {
        int i, j, ncells;
            int id1,id2;
        unpackIndices(iGlob,dom.ny+2*hc,dom.nx+2*hc,j,i);
                if(i>hc-2 && i<dom.nx+hc && j>hc-1 && j<dom.ny+hc){
                        ncells=dom.ncells;
```

```
                        id1=iGlob ;
                        id2=j *(dom . nx+2*hc )+ i +1;
                        // computationally intensive code to compute fluxes at the edge between cells id1 and id2
            }
        }
```

## 4   Verification and validation

In this section we report evidence supporting the claim that SERGHEI-SWE is an accurate, robust and efficient shallow water solver. The formal accuracy testing strategy is based on several well-known benchmark cases with well-defined reference solutions. Herein, for brevity, we focus only on the results of these tests, while providing a minimal presentation of the setups. We refer the interested reader to the original publications (and to the many instances in which these tests have been used) for further details on the geometries, parametrisations and forcing.

We purposely report an extensive testing exercise to show the wide applicability of SERGHEI across hydraulic and hydrological problems, with a wide range of the available benchmark tests. Analytical, experimental and field-scale tests are included. The first are aimed at showing formal convergence and accuracy. The experimental cases are meant as validation of the capabilities of the model to reach physically meaningful solutions under a variety of conditions. The field-scale tests showcase the applicability of the solver for real problems, and allow for strenuous computational tasks to show performance, efficiency and parallel-scaling. All solutions reported here were computed using double precision arithmetic.

### 4.1   Analytical steady flows

We test SERGHEI's capability to capture moving equilibria in a number of steady flow test cases compiled in (Delestre et al., 2013). Details of the test cases for reproduction purposes can be retrieved from (Delestre et al., 2013) and the accompanying software SWASHES—in this work, we use SWASHES version 1.03. In the following test cases, the domain is always discretised using 1000 computational cells. A summary of $L$-norms for all test cases is given in Table 2. The definition of the $L$-norms is given in Appendix A.

| Case | $L_1$ (m) | $L_2$ (m) | $L_\infty$ (m) |
|---|---|---|---|
| Figure 4 | 0.0 | 0.0 | 0.0 |
| Figure 5(left) | 0.68584 | 0.01909 | 0.0015 |
| Figure 5(right) | 1.02096 | 0.06826 | 0.0622 |

**Table 2.** Analytical steady flows: Summary of $L$-norms for errors in water depth; $L$-norms for errors in unit discharge are in the range of machine accuracy and omitted here.
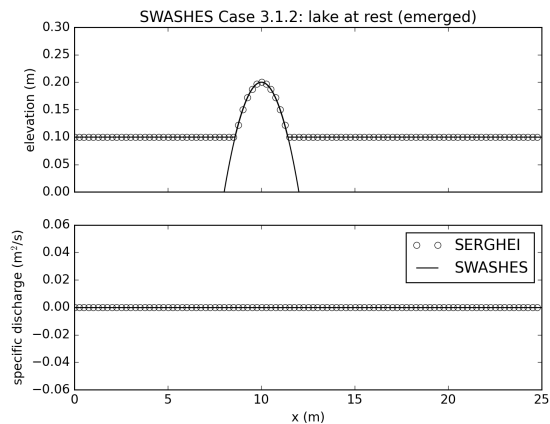
**11**

**Figure 4.** Lake at rest solution for emerged bump. SERGHEI-SWE satisfies the C-property

### 4.1.1 C-property

These tests feature a smooth bump in a one-dimensional, frictionless domain which can be used to validate the C-property,
well-balancing, and the shock-capturing ability of the numerical solver (Morales-Hernández et al., 2012; Murillo and García-
Navarro, 2012). Figure 4 shows that SERGHEI-SWE satisfies the C-property by preserving a *lake-at-rest* in the presence of
emerged bump (an immersed bump test is shown in Section A1) and matches the analytical solution provided by SWASHES.

### 4.1.2 Well-balancing

To show well-balancing under steady flow, we computed two transcritical flows, based on the analytical benchmark of a one-
dimensional flume with varying geometry proposed by MacDonald et al. (1995). These tests are well-known and widely used as
benchmark solutions (e.g., Caviedes-Voullième and Kesserwani, 2015; Delestre et al., 2013; Kesserwani et al., 2019; Morales-
Hernández et al., 2012; Murillo and García-Navarro, 2012). Additional well-balancing tests can be found in Section A2. At
steady state, local acceleration terms and source terms balance each other out such that the free surface water elevation becomes
a function of bed slope and friction source terms. Thus, these test cases can be used to validate the implementation of these
source terms and the well-balanced nature of the complete numerical scheme. This is particularly important to subcritical
fluvial flows, and rainfall-runoff problems, since both usually dominated by these two terms.

Figure 5 shows comparisons between SERGHEI-SWE and analytical solutions (obtained through SWASHES) for two tran-
scritical steady flows. Very good agreement is obtained. Note that the unit discharge is captured with machine accuracy in the
presence of friction and bottom changes, which is mainly due to the upwind friction discretization used in the SERGHEI-SWE
solver. As reported by Burguete et al. (2008); Murillo et al. (2009), a centered friction discretization does not ensure a perfect
balance between fluxes and source terms for steady states even if using the improved discretisation by Xia et al. (2017).
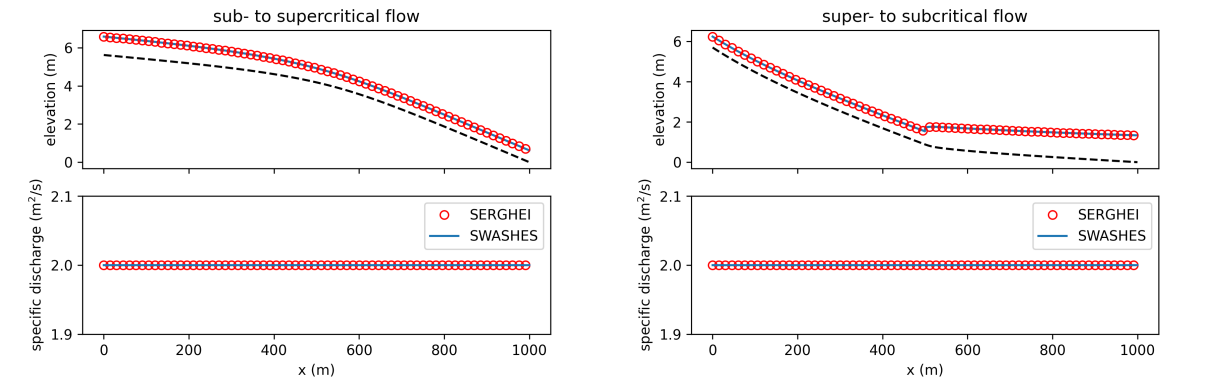
**12**

**Figure 5.** Analytical steady flows: Flumes. SERGHEI-SWE captures moving equilibria solutions for two transcritical steady flows. Note that the solution is stable (no oscillations) and well-balanced (discharge remains constant along the flume).

## 4.2 Analytical dam break

We verify SERGHEI-SWE's capability to capture transient flow based on analytical dam breaks (Delestre et al., 2013). Dam break problems are defined by an initial discontinuity in the water depth in the domain $h(x)$, such that

$$h(x) = \begin{cases} h_L & \text{if } x \leq x_0, \\ h_R & \text{otherwise,} \end{cases} \tag{5}$$

where $h_L$ denotes a specified water depth on the left hand-side of the location of the discontinuity $x_0$ and $h_R$ denotes the specified water depth on the right hand-side of $x_0$. The domain is $10\,\mathrm{m}$ long, the discontinuity is located at $x_0 = 5\,\mathrm{m}$, and the total run time is $6\,\mathrm{s}$. Initial velocities are nil in the entire domain. In the following, we report empirical evidence of the numerical schemes mesh convergence property by comparing model predictions for test cases with 100, 1000, 10000, and 100000 elements, respectively.

A classical frictionless dam-break over a wet bed is reported in Section A3. Here we focus on a frictionless dam break over a dry bed. Flow featuring depth close to dry bed is a special case for the numerical solver, because regular wave speed estimations become invalid Toro (2001). Initial conditions are set as $h_L = 0.005\,\mathrm{m}$ and $h_R = 0\,\mathrm{m}$. Model results are plotted against the analytical solution by Ritter for different grid resolutions in Figure 6. The model results converge to the analytical solution as the grid is refined. This is also seen in Table 3, where errors and convergence rates for this test case are summarised. Note that the norms definition can be found in Section A2. The observed convergence rate is below the theoretical convergence rate of $R = 1$, because of the increased complexity introduced by the discontinuity in the solution and the presence of dry bed.
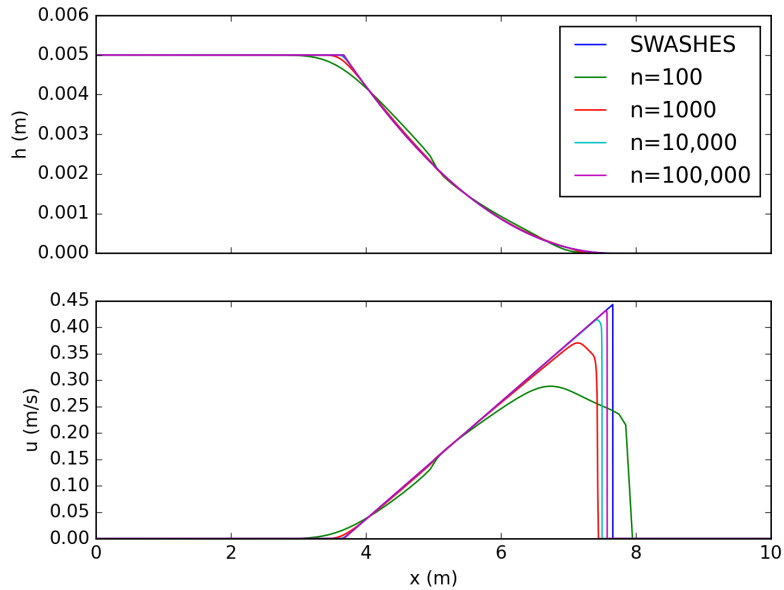
**13**

**Figure 6.** Dam break on dry bed without friction: Model predictions for different number of grid cells. SERGHEI-SWE converges to the analytical solution (Ritter's solution) as the grid is refined.

| n | $L1(h)$ (m) | $L2(h)$ (m) | $R(h)$ (m) | $L1(u)$ (m/s) | $L2(u)$ (m/s) | $R(u)$ (m/s) |
|---|---|---|---|---|---|---|
| 100 | 0.01566 | 0.02343 | - | 0.23 | 0.526 | - |
| 1000 | 0.00396 | 0.00645 | 0.6 | 0.138 | 0.4053 | 0.22 |
| 10000 | 0.00068 | 0.00137 | 0.76 | 0.08169 | 0.34 | 0.22 |
| 100000 | 0.0001 | 0.00026 | 0.83 | 0.04193 | 0.248 | 0.28 |

**Table 3.** Analytical dam break: L-norms and empirical convergence rates (R) for water depth ($h$) and velocity ($u$)

### 4.3 Analytical oscillation: parabolic bowl

We present transient two-dimensional test cases with moving wet-dry fronts that consider the periodical movement of water in a parabolic bowl, so-called *oscillations* that have been studied by Thacker (1981). We replicate two cases from the SWASHES compilation (Delestre et al., 2013), using a mesh spacing of $\Delta x = 0.01\,\text{m}$, one reported here and the other in Section A4.

The well-established test case by Thacker (1981) for a periodic oscillation of a planar surface in a frictionless paraboloid has been extensively used for validation of shallow water solvers (e.g., Aureli et al., 2008; Dazzi et al., 2018; Liang et al., 2015; Murillo and García-Navarro, 2010; Vacondio et al., 2014; Zhao et al., 2019), because of its rather complex 2D nature and the presence of moving wet/dry fronts. The topography is defined as

$$z(r) = -h_0 \left( 1 - \frac{r^2}{a^2} \right), \qquad r = \sqrt{(x - L/2)^2 + (y - L/2)^2}, \tag{6}$$

where $r$ is the radius, $h_0$ is the water depth at the centre of the paraboloid, $a$ is the distance from the centre to the zero elevation shoreline, $L$ is the length of the square-shaped domain, and $x$ and $y$ denote coordinates inside the domain. The analytical solution is derived in (Thacker, 1981). We use the same values as Delestre et al. (2013), that is $h_0 = 0.1\,\text{m}$, $a = 1\,\text{m}$, and $L = 4\,\text{m}$. The simulation is run for 3 periods ($T = 2.242851\,\text{s}$), with a spatial resolution of $\delta x = 0.01\,\text{m}$. The analytical solution can be found in (Thacker, 1981; Delestre et al., 2013).

Snapshots of the simulation are plotted in Figure 7 and compared to the analytical solution. The model results agree well with the analytical solution after three periods, with slightly growing phase error, as is commonly observed on this test case.

### 4.4 Variable rainfall over a sloping plane

Govindaraju et al. (1990) presented an analytical solution to a time-dependent rainfall over a sloping plane, which is commonly used (Caviedes-Voullième et al., 2020a; Gottardi and Venutelli, 2008; Singh et al., 2015). The plane is $21.945\,\text{m}$ long, with a slope of $0.04$. We select rainfall B from Govindaraju et al. (1990), a piecewise constant rainfall with two periods of alternating low and high intensities (50.8 and 101.6 $\text{mmh}^{-1}$) up until $2400\,\text{s}$. Friction is modeled with Chezy's equation, with a roughness coefficient of $1.767\,\text{m}^{1/2}\text{s}^{-1}$. The computational domain was defined by a $200 \times 10$ grid, with $\delta x = 0.109725\,\text{m}$.

The simulated discharge hydrograph at the outlet is compared against the analytical solution in Figure 8. The numerical solutions matches the analytical one very well. The only relevant difference occurs in the magnitude of the second discharge peak, which is slightly underestimated in the simulation.

## 5 Laboratory-scale experiments

### 5.1 Experimental steady and dam-break flows over complex geometry

Martínez-Aranda et al. (2018) presented experimental results of steady and transient flows over several obstacles, while recording transient 3D water surface elevation in the region of interest. We selected the so-called G3 case, and simulated both a
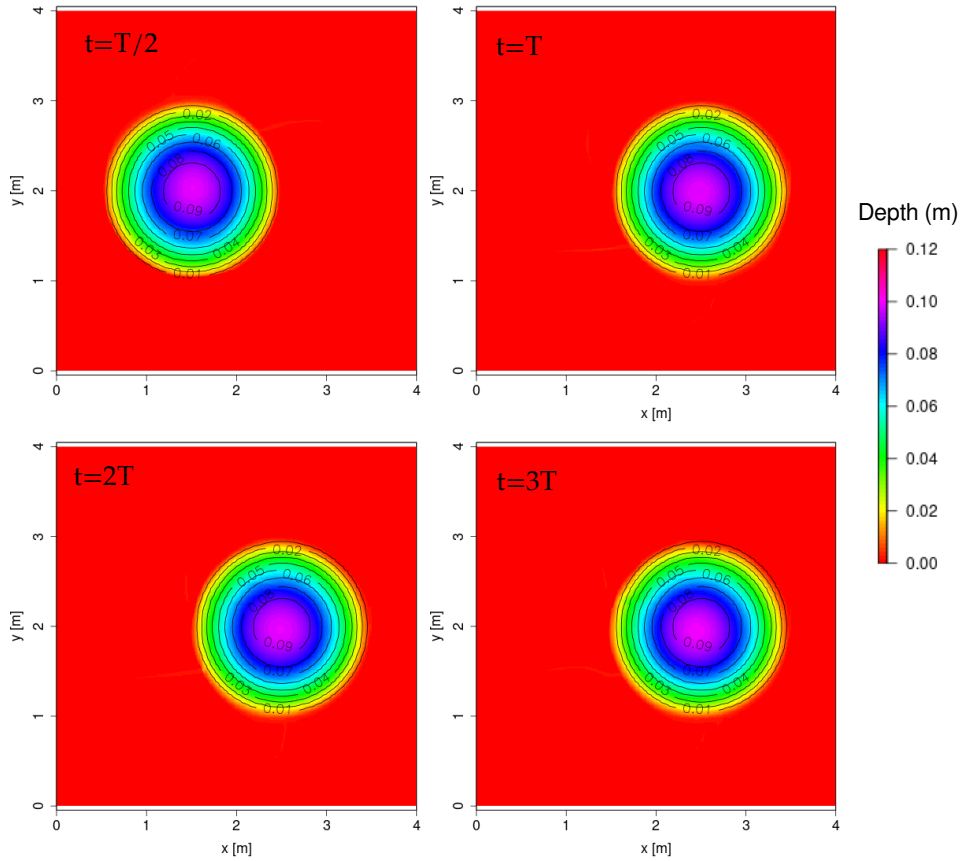
**Figure 7.** Planar surface in a paraboloid: Snapshots of water depth by the model compared to the analytical solution (contour lines). Period $T = 2.242851\,\mathrm{s}$

dam-break and steady flow. The experiment took place in a double-sloped plexiglass flume, $6\,\mathrm{m}$ long, and $24\,\mathrm{cm}$ wide. The obstacles in this case are a symmetric contraction and a rectangular obstacle on the centerline, downstream of the contraction.

For both cases the flume (including the upstream wider reservoir) was discretised at a $5\,\mathrm{mm}$ resolution, resulting in a computational domain with 106887 cells. Manning's roughness was set to $0.01\,\mathrm{s\,m^{-1/3}}$. The steady simulation was run from an initial state with uniform depth $h = 5\,\mathrm{cm}$ up to $t = 300\,\mathrm{s}$. The dam-break simulation duration was $40\,\mathrm{s}$.

The steady flow case had a discharge of $2.5\,\mathrm{L/s}$. Steady water surface results in the obstacle region are shown in Figure 9, for a centerline profile ($y = 0$) and a cross section at the rectangular obstacle, specifically at $x = 2.40\,\mathrm{m}$ (the coordinate system is set at the center of the flume inlet gate). The simulation results approximate experimental results well. The mismatches are similar to those analysed by Martínez-Aranda et al. (2018) and can be attributed to turbulent and 3D phenomena near the obstacles.

**16**
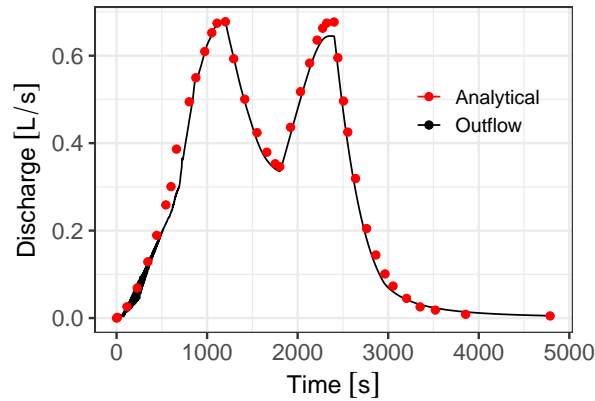
**Figure 8.** Simulated and analytical discharge for the analytical case of rainfall in a flume

The dam-break case is triggered by a sudden opening of the gate followed by a wave advancing along the dry flume. Results for this case at three gauge points are shown in Figure 10. Again, the simulations approximate experiments well, capturing both the overall behaviour of the water depths and the arrival of the dam break wave, with local errors attributable to the violent dynamics (Martínez-Aranda et al., 2018).

360
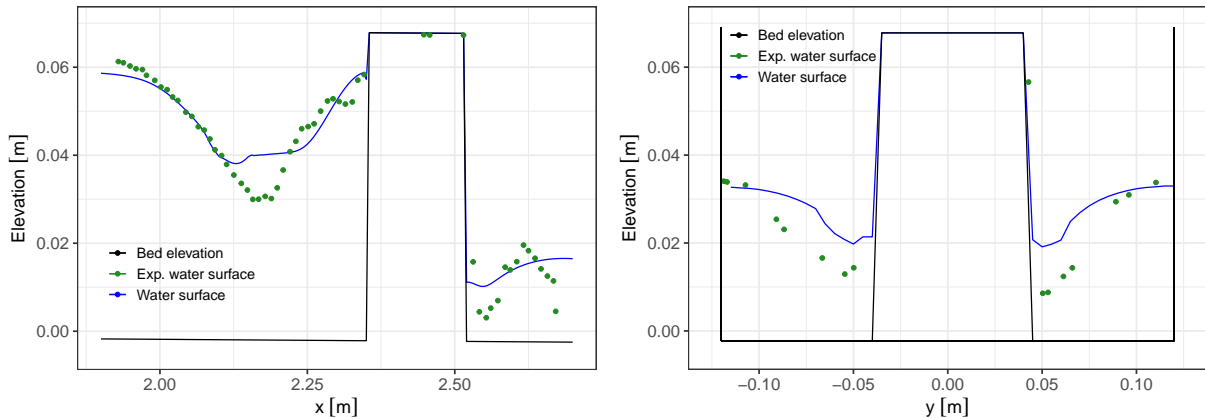


**Figure 9.** Simulated and experimental steady water surface in the obstacle region of the G3 flume for the center line profile $y = 0\,\mathrm{m}$ (left) and a cross-section $x = 2.40\,\mathrm{m}$ (right)

## 5.2 Experimental unsteady flow over an island

Briggs et al. (1995) presented an experimental test of an unsteady flow over a conical island. This test has been extensively used for benchmarking (Bradford and Sanders, 2002; Choi et al., 2007; García-Navarro et al., 2019; Hou et al., 2013b; Liu et al., 1995; Lynett et al., 2002; Nikolos and Delis, 2009). A truncated cone of base diameter $7.2\,\mathrm{m}$, top diameter $2.2\,\mathrm{m}$ and $0.625\,\mathrm{m}$
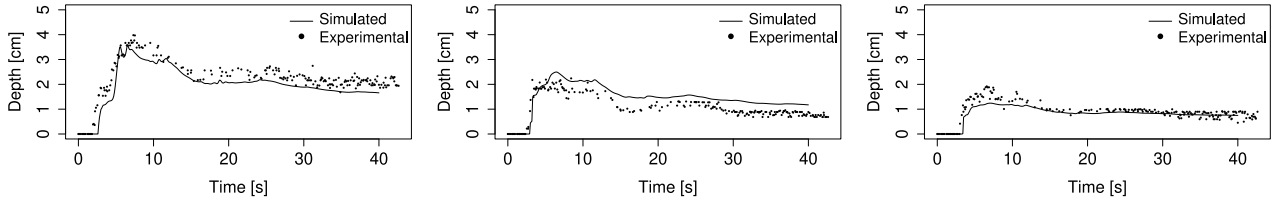
**Figure 10.** Simulated and experimental transient water depths at three gauge points (left $x = 2.25\,\mathrm{m}$, $y = 0\,\mathrm{m}$; center $x = 2.40\,\mathrm{m}$, $y = 0.08\,\mathrm{m}$; right $x = 2.60\,\mathrm{m}$, $y = 0\,\mathrm{m}$) for the G3 flume dam-break over several obstacles.

high, was placed at the centre of a $26 \times 27.6\,\mathrm{m}$ smooth and flat domain. An initial hydrostatic water level of $h_0 = 0.32\,\mathrm{m}$ was set, and a wave was imposed on the boundary following

$$h_b = h_0 + A\,\mathrm{sech}^2\left(\frac{B(t-T)}{C}\right) \tag{7}$$

$$B = \sqrt{gh_0}\left(1 + \frac{A}{2h_0}\right) \tag{8}$$

$$C = h_0\sqrt{\frac{4h_0 B}{3A\sqrt{gh_0}}} \tag{9}$$

where $A = 0.032m$ is the wave amplitude and $T = 2.84s$ is the time at which the peak of the wave enters the domain. Figure 11 shows results for a simulation with a $2.5\,\mathrm{cm}$ resolution, resulting in 1.2 million cells. A roughness coefficient of $0.013\,\mathrm{sm}^{-1/3}$ was used for the concrete surface. The results are comparable to previous solutions in the literature, in general reproducing well the water surface surface, with some delay over experimental measurements.
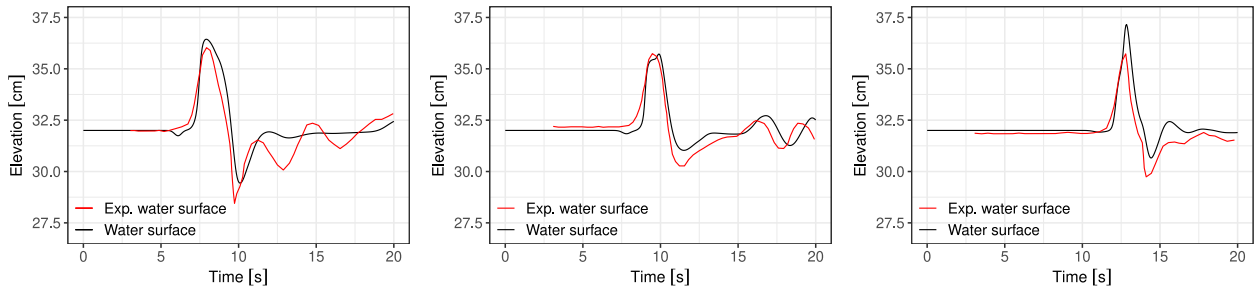


**Figure 11.** Simulated and experimental results of unsteady flow over an island for gauges G9 (left), G16 (centre) and G22 (right)

## 5.3 Experimental rainfall-runoff over an idealised urban area

Cea et al. (2010a) presented experimental and numerical results for a range of laboratory scale rainfall-runoff experiments on an impervious surface with different arrangements of buildings, which have been frequently used for model validation (Caviedes-Voullième et al., 2020a; Cea et al., 2010b; Cea and Bladé, 2015; Fernández-Pato et al., 2016; Su et al., 2017; Xia

**18**

et al., 2017). This laboratory scale test includes non-trivial topographies, small water layers and wetting/drying fronts, making it a good benchmark for realistic rainfall-runoff conditions.

380    The dimensions of the experimental flume are $2 \times 2.5\,m$. Here, we select one building arrangement named A12 by Cea et al. (2010a). The original DEM is available (from Cea et al. (2010a)) at a resolution of $1\,cm$. The buildings are $20\,cm$ high, and are represented as topographical features on the domain. All boundaries are closed, except for the free outflow at the outlet. The domain was discretised with a $\delta x = 1\,cm$ resolution, resulting in $54600$ cells. The domain was forced by two constant pulses of rain of $85\,mmh^{-1}$ and $300\,mmh^{-1}$ (lowest and highest intensities in the experiments) with a duration of $60\,s$ and $20\,s$. The

385    simulation was run up to $t = 200\,s$. Friction was modelled by Manning's equation, with a constant roughness coefficient of $0.010\,sm^{-1/3}$ for steel (Cea et al., 2010a).

Figure 12 shows the experimental and simulated outflow discharge for both rainfall pulses. There is a very good qualitative agreement, and peak flow is quantitatively well reproduced by the simulations. For the $300\,mmh^{-1}$ intensity rainfall, the onset of runoff is earlier than in the experiments, and overall the hydrograph is shifted towards earlier times. Cea et al. (2010a)

390    observed a similar behaviour, and pointed out that this is likely caused by surface tension during the early wetting of the surface, and it was most noticeable on the experiments with higher rainfall intensity.
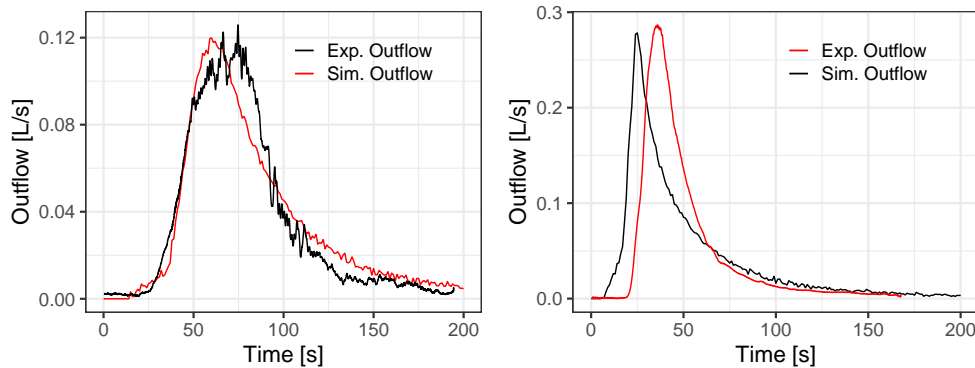


**Figure 12.** Simulated hydrographs compared to experimental data from Cea et al. (2010a) for two rainfall pulses on the A12 building arrangement. Left: rain intensity $85\,mmh^{-1}$, duration $60\,s$. Right: rain intensity $300\,mmh^{-1}$, duration $20\,s$

## 6    Plot-scale to catchment-scale experiments

### 6.1    Plot-scale field rainfall-runoff experiment

Tatard et al. (2008) presented a rainfall-runoff plot-scale experiment performed in Thies, Senegal. This test has been often used

395    for benchmarking of rainfall-runoff models (Caviedes-Voullième et al., 2020a; Chang et al., 2016; Mügler et al., 2011; Özgen-Xian et al., 2020; Park et al., 2019; Simons et al., 2014; Yu and Duan, 2017; Weill, 2007). The domain is a field plot of $10 \times 4\,m$, with an average slope of $0.01$. A rainfall simulation with an intensity of $70\,mmh^{-1}$ during $180\,s$ was performed. Steady velocity

measurements were taken at 62 locations. The Gauckler-Manning roughness coefficient was set to $0.02 \, \mathrm{s m}^{-1/3}$ and a constant infiltration rate was set to $0.0041667 \, \mathrm{mm s}^{-1}$ (Mügler et al., 2011). The domain was discretised with $\delta x = 0.02666 \, \mathrm{m}$, resulting is 56250 cells, with a single free outflow boundary downslope.

Simulated velocities are compared to experimental velocities at the 62 gauged locations in Figure 13. A good agreement of simulated and experimental velocities exists, especially in the lower velocity range. The agreement is similar to previously reported results (e.g., Caviedes-Voullième et al., 2020a), and the differences between simulated and observed velocities have been shown to be a limitation of a depth-independent roughness and Manning's model (Mügler et al., 2011).
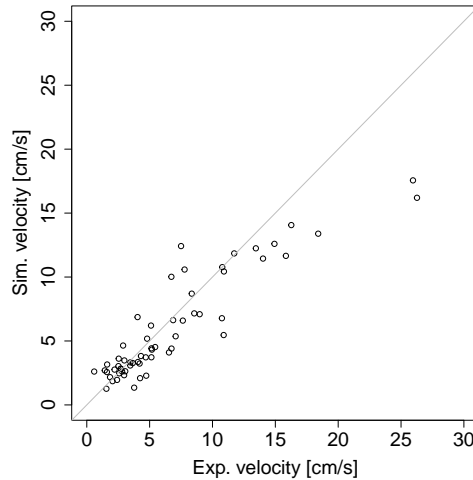


**Figure 13.** Comparison of simulated (line) and experimental (circles) steady velocities in the Thies field case.

## 6.2 Malpasset dam-break

The Malpasset dam-break event (Hervouet and Petitjean, 1999) is the most commonly used real-scale benchmark test in shallow water modelling (An et al., 2015; Brodtkorb et al., 2012; Brufau et al., 2004; Caviedes-Voullième et al., 2020b; Duran et al., 2013; George, 2010; Hervouet and Petitjean, 1999; Hou et al., 2013a; Kesserwani and Liang, 2012; Kesserwani and Sharifian, 2020; Kim et al., 2014; Liang et al., 2007; Sætra et al., 2015; Schwanenberg and Harms, 2004; Smith and Liang, 2013; Valiani et al., 2002; Xia et al., 2011; Yu and Duan, 2012; Wang et al., 2011; Zhou et al., 2013; Zhao et al., 2019). Although it may not be particularly challenging for current solvers, it remains an interesting case due to its scale, and the available field and experimental data (Aureli et al., 2021). The computational domain was discretised to $\delta x = 25 \, \mathrm{m}$ and $\delta x = 10 \, \mathrm{m}$ (resulting in 83137 and 515262 cells respectively). The Gauckler-Manning coefficient was set to a uniform value of $0.033 \, \mathrm{s m}^{-1/3}$, which has been shown to be a good approximation in the literature. Figure 14 shows a comparison of simulated water surface elevation (WSE) and arrival time for two resolutions against the reference experimental and field data. Figure 15 shows the geospatial distribution of the relative WSE error, and the ratio of the simulated arrival time to the observed time. Overall, WSE shows a

good agreement and somewhat smaller scatter for the higher resolution. Arrival time tends to be overestimated, and somewhat more for coarser resolutions.
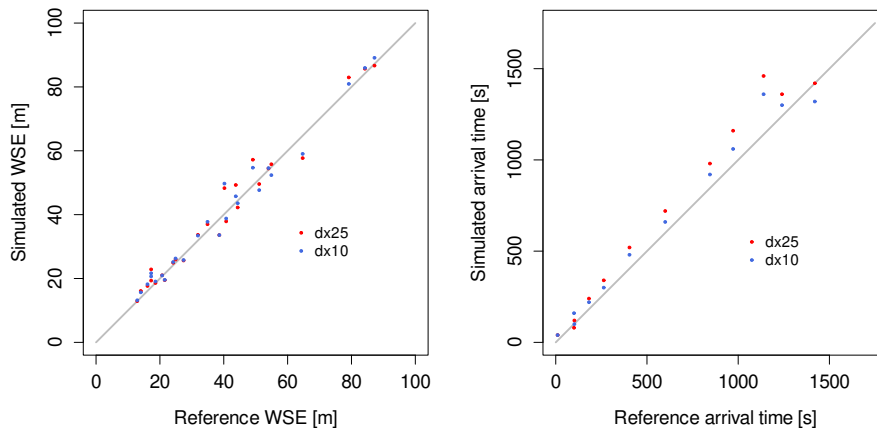


**Figure 14.** Water surface elevations (left) and arrival time (right) result comparison for two meshes of the Malpasset case.
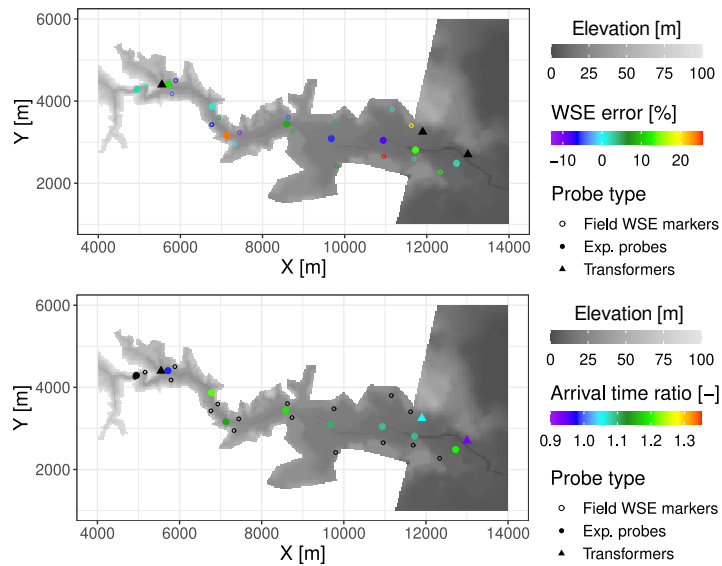


**Figure 15.** Geolocated relative WSE error (top) and ratio of arrival time (bottom) for the Malpasset dam-break test case with $\delta x = 10\,\mathrm{m}$.

# 7 Performance and scaling

420    In this section we report an investigation of the computational performance and parallel scaling of SERGHEI-SWE for selected test cases. To demonstrate performance-portability, we show performance metrics for both OpenMP and CUDA backends enabled by Kokkos, computed on CPU and GPU architectures respectively. For that, hybrid MPI-OpenMP and MPI-CUDA implementations are used, with one MPI task per node for MPI-OpenMP and one MPI task per GPU for MPI-CUDA. Most of the runs were performed on JUWELS at JSC (Jülich Supercomputing Centre). Additional HPC systems were also used for

425    come cases. Properties of all systems are shown in Table 4. Additionally, we provide performance metrics on non-HPC systems including some consumer-grade GPUs.

   It is important to highlight that no performance tuning or optimisation has been carried out for these tests, and that no system-specific porting efforts were done. All runs relied entirely on Kokkos for portability. The code was simply compiled with the available software stacks in the HPC systems and executed. All results reported here were computed using double

430    precision arithmetic.

**Table 4.** HPC systems in which SERGHEI-SWE has been tested

| Name | Centre | Institution | Country | Devices | Vendor | Device/node | Nodes |
| --- | --- | --- | --- | --- | --- | --- | --- |
| | | | | Xeon Platinum 8168 CPU | Intel | 2x(2x24) | 2567 |
| JUWELS | JSC | FZJ | Germany | Volta V100 GPU | Nvidia | 4 | 56 |
| | | | | Ampere A100 GPU | Nvidia | 4 | 936 |
| JURECA-DC | JSC | FZJ | Germany | EPYC 7742 2.25 GHz | AMD | 2x(2x64) | 480 |
| Summit | OLCF | ORNL | USA | Volta V100 GPU | Nvidia | 6 | 4608 |
| Cori | NERSC | LBNL | USA | Xeon E5-2698 v3 CPU | Intel | 32 | 2388 |

JSC: Jülich Supercomputing Centre; FZJ: Forschungszentrum Jülich

OLCF: Oak Ridge Leadership Computing Facility; ORNL: Oak Ridge National Laboratory

NERSC: National Energy Research Scientific Computing Center; LBNL: Lawrence Berkeley National Laboratory

## 7.1 Single node scaling – Malpasset dam-break

The commonly used Malpasset dam-break test (introduced in Section 6.2) was also tested for computational performance at a resolution of $\delta x = 10\,\mathrm{m}$. Results are shown in Figure 16. The case was computed on CPUs a single JUWELS node and a single JURECA-DC node. Three additional runs with single Nvidia GPUs were carried out: a commercial-grade GeForce RTX 3070,

435    8GB GPU (in a desktop computer) and two scientific-grade cards V100 and A100 respectively (in JUWELS). As Figure 16 shows, CPU runtime quickly approaches an asymptotic behaviour (therefore demonstrating that additional nodes are not useful in this case). Notably, all three GPUs outperform a single CPU node, and the performance gradient among the GPUs is evident. The A100 GPU is roughly 6.5 faster than a full JUWELS CPU node, and even for the consumer-grade RTX 3070 the speed-up compared to a single HPC node is 2.2. Although it is possible to scale up this case with significantly higher resolution and test

440    it with multiple GPUs, it is not a case well suited for such a scaling test. Multiple GPUs (as well as multiple nodes with either

CPUs or GPUs) require a domain decomposition. The orientation of the Malpasset domain is roughly NW-SE, which makes both 1D decompositions (along $x$ or $y$) and 2D decompositions ($x$ and $y$) inefficient, as many regions have no computational load. Moreover, the dam-break nature of the case implies that a large part of the valley is dry for long periods of time, therefore load balancing among the different nodes/GPUs will be poor.
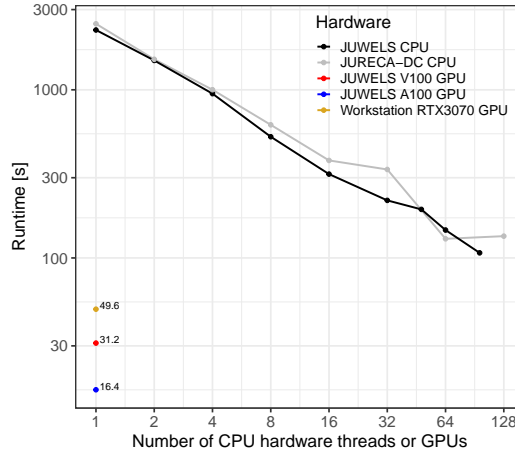


**Figure 16.** Scaling for the Malpasset case ($\delta x = 10\,\mathrm{m}$) on a single node and on single GPUs. GPU speed-ups relative to a full JUWELS node are 6.5 (A100), 3.4 (V100) and 2.2 (RTX 3070).

## 7.2 HPC scaling – 2D circular dam break case

This is a simple analytical verification test in the shallow water literature, which generalises the 1D dam-break solution. We purposely select this case (instead of one of the many verification problems) for its convenience for scaling studies. Firstly, resolution can be increased as will. Additionally, the square domain allows for trivial domain decomposition, which together with the fully wet domain and the radially-symmetric flow field minimises load balancing issues. Essentially, it allows for a very clean scalability test with minimal interference from the problem topology, which facilitates scalability and performance analysis (in contrast to the limitations of the Malpasset domain discussed in Section 7.1). We take a $400 \times 400\,\mathrm{m}$ flat domain with center at $(0,0)$ and initial conditions given by

$$h(x,y,t=0) = \begin{cases} 4 & \text{if } \sqrt{x^2 + y^2} \leq 50 \\ 1 & \text{otherwise} \end{cases} \tag{10}$$

We generated three computational grids, with $\delta x = 0.05, 0.025, 0.0175\,\mathrm{m}$, which correspond to 64, 256 and 552 million cells respectively. Figure 17 shows the strong scaling results for the 64 and 256 million cells cases, computed in the JUWELS-booster system, on A100 Nvidia GPUs. The 64 million does not scale well beyond 4 GPUs. However, the 256 cells problem scales well up to 64 GPUs (and efficiency starts to decrease with 128), showing that the first case simply is too small for significant gains.
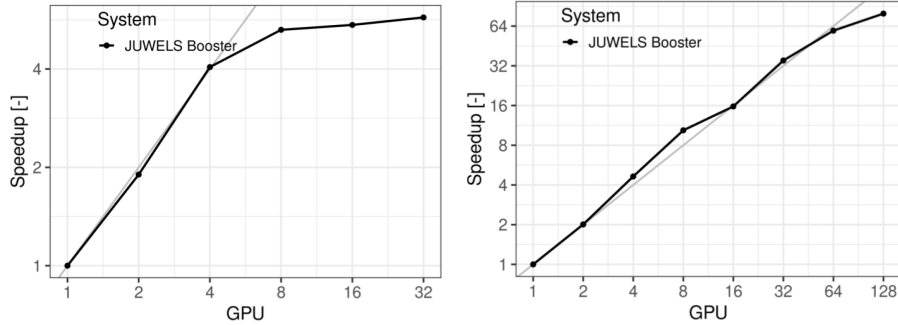
**Figure 17.** Strong scaling behaviour for a circular dam break test case with two resolutions. Left: $\delta x = 0.05$, 64 million cells. Right: $\delta x = 0.025$, 256 million cells.

For the $552$ million cell grid, only two runs were computed with 128 and 160 GPUs (corresponding to 32 and 40 nodes in
JUWELS-booster respectively). Runtime for these was $95.4$ and $84.7\,$s respectively, implying a very good $89\%$ scaling effi-
ciency for this large number of GPUs. For this problem and these resources, the time required for inter-GPU communications
is comparable to that used by kernels computing fluxes and updating cells, signalling scalability limits for this case on the
current implementation.

### 7.3 HPC-scaling of rainfall-runoff in a large catchment

To demonstrate scaling under production conditions of real scenarios, we use an idealised rainfall-runoff simulation over the
Lower Triangle region in the East River Watershed (Colorado, USA) (Carroll et al., 2018; Hubbard et al., 2018; Özgen-Xian
et al., 2020). The domain has an area of $14.82\,km^2$, and elevations ranging from $2759 - 3787\,m$. The computational problem is
defined with a resolution of $\delta x = 0.5\,$m (matching the highest resolution DEM available), resulting in $122 \times 10^6$ computational
cells. Although this is not a particularly large catchment, the very high resolution DEM available makes it an interesting
performance benchmark, which is the sole interest for it in this paper.

For practical purposes, two configurations have been used for this test. A short rainfall of $T = 870\,$s, which was computed in
Cori and JUWELS to assess CPU performance and scalability (results shown in Figure 18). A long rainfall event lasting $T = 12000\,$s was simulated in Summit and JUWELS to assess GPU performance and scalability, with results shown in Figure 19.
CPU results (Figure 18) show that the strong scaling behaviour in Cori and JUWELS is very similar. Absolute runtimes are
longer for Cori since the scaling study was carried starting from a single core, whereas in JUWELS it was with a full node (i.e.,
48 cores). Most importantly, the GPU strong scaling behaviour overlaps almost completely between JUWELS and Summit,
although computations in Summit were somewhat faster. CPU and GPU scaling is clearly highly efficient and with similar
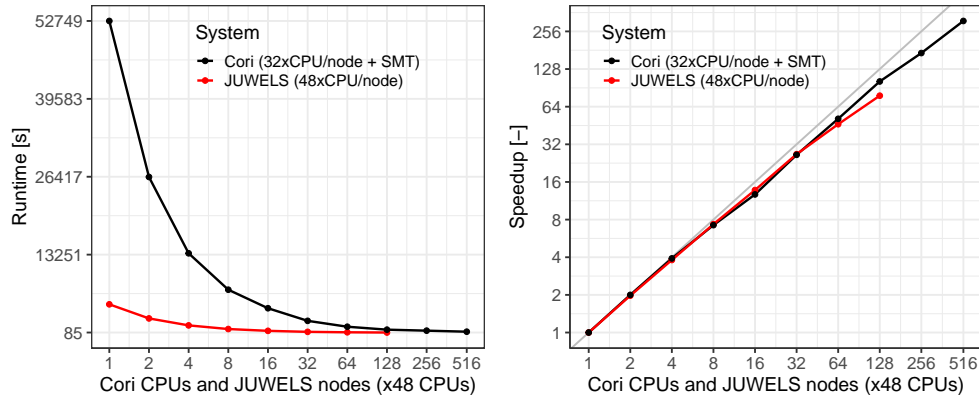behaviour. These results demonstrate the performance-portability delivered via Kokkos to SERGHEI.

**Figure 18.** Runtime (left) and speed-up (right) for a strong scaling experiment with SERGHEI-SWE using CPUs on Cori and JUWELS for the short rainfall event. See Table 4 for details on the systems.
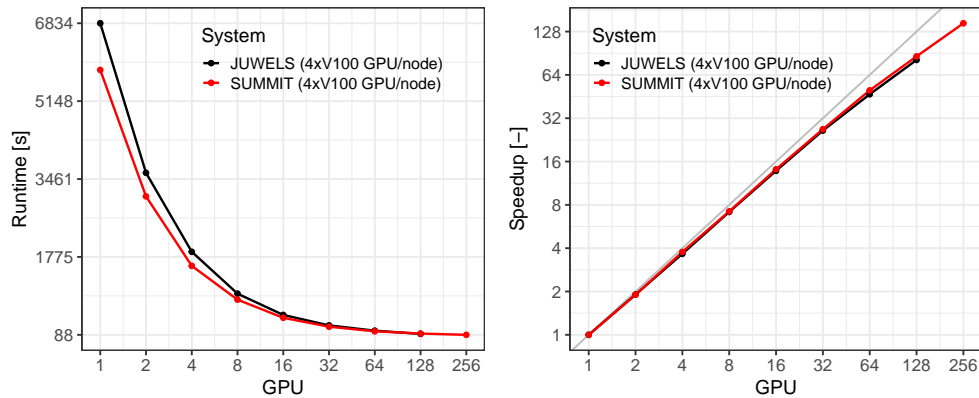


**Figure 19.** Runtime (left) and speed-up (right) for a strong scaling experiment with SERGHEI-SWE using GPUs on Summit and JUWELS for the long rainfall event. See Table 4 for details on the systems.

## 8   Conclusions and outlook

480   In this paper we present the SERGHEI framework, and in particular the SERGHEI-SWE module. SERGHEI-SWE implements a 2D fully dynamic shallow water solver, harnessing state-of-the-art numerics, and leveraging on Kokkos to facilitate portability across architectures. We show through empirical evidence with a large set of well established benchmarks that SERGHEI-SWE is accurate, numerically stable, and robust. Importantly, we show that SERGHEI-SWE's parallel scaling is very good for CPU-based HPC systems, consumer-grade GPUs, and GPU-based HPC systems. Consequently, we claim that SERGHEI is indeed

485   performance-portable, and approaching exascale-readiness. These features make SERGHEI-SWE a plausible community code for shallow water modelling for a wide range of applications requiring large scale, very high resolution simulations.

Exploiting increasingly better and highly resolved geospatial information (DEMs, land use, vector data of structures) prompts the need for high resolution solvers. At the same time, the push towards the study of multiscale systems and integrated management warrants for increasingly larger domains. Together, these trends result in larger computational problems, motivating the need for exascale-ready shallow water solvers. Additionally, HPC technology is evermore available, not only via (inter)national research facilities, but also through cloud computing facilities. It is arguably timely to enable such an HPC ready solver.

The HPC allows not only for large simulations, but also large ensembles of simulations allowing to address uncertainty issues and scenario analysis for engineering problems, and parameter space exploration and hypothesis testing. Furthermore, although the benefits of high resolution may be marginal for runoff hydrograph estimations, they allow to better resolve the local dynamics in the domain. Flow paths, transit times, wetting/drying dynamics, and connectivity play important roles in transport and ecohydrological processes. For these purposes, enabling very high resolution simulations will prove highly beneficial. We also envision that, provided sufficient computational resources, SERGHEI-SWE could be used for operational flood forecasting and probabilistic flash flood modelling. Altogether, this strongly paves the way for the uptake of shallow water solvers by the broader ESM community and its coupling to Earth system models, and their many applications from process and system understanding, to hydrometeorological risk and impact assessment. We also envision that, for users not requiring HPC capabilities, the benefit of SERGHEI-SWE is access to a transparent, open-sourced, performance-portable software that allows to exploit workstation GPUs efficiently.

As additional SERGHEI modules become operational, the HPC capabilities will further enable simulations unfeasible with the current generation of available solvers. For example, with a fully operational transport and morphology module, it will be possible to run decade-long morphological simulations relevant for river management applications; to better capture sediment connectivity and sediment cascades across the landscape, a relevant topic for erosion and catchment management; or to perform catchment-scale hydro-biogeochemical simulations with unprecedented high spatial resolution for better understanding of ecohydrological and biogeochemical processes.

Finally, SERGHEI is conceptualised and designed with extendibility and software interoperability in mind, with design choices made to facilitate foreseeable future developments on a wide range of topics, such as: (i) numerics, e.g., the Discontinuous Galerkin discretisation strategies (Caviedes-Voullième and Kesserwani, 2015; Shaw et al., 2020) and multiresolution adaptive meshing (Caviedes-Voullième et al., 2020b; Kesserwani and Sharifian, 2020, 2022; Özgen-Xian et al., 2020); (ii) interfaces to mature geochemistry engines, e.g., CrunchFlow (Steefel, 2009) and PFLOTRAN (Lichtner et al., 2015), and (iii) vegetation models with varying degree of complexity, for example, Ecosys (e.g. Grant et al., 2007; Grant and the Ecosys development team, 2022), EcH2O (Maneta and Silverman, 2013).

A repository containing test cases is available https://gitlab.com/serghei-model/serghei_testcases. This repository contains many of the cases reported here, except those for which we cannot publicly release data, but which can be obtained from the original authors of the datasets. A static version of this datasets is archived in Zenodo, with DOI: 10.5281/zenodo.7041392.

Additional convenient pre- and postprocessing tools are also available at https://gitlab.com/serghei-model/sergheir.

*Author contributions.* DCV: Conceptualisation, Investigation, Software, Validation, Visualisation, Writing. MMH: Conceptualisation, Methodology, Software, Formal analysis, Writing. MN: Software. IOX: Formal Analysis, Software, Validation, Visualisation, Writing.

*Competing interests.* The authors declare no conflicts of interests.

## Glossary

**CFL** Courant-Friederich-Lewy.

**Cori** Cori supercomputer at the National Energy Research Scientific Computing Center (USA).

**CPU** Central Processing Unit.

**CUDA** Compute Unified Device Architecture, programming interface for Nvidia GPUs.

**El Capitan** El Capitan supercomputer at the Lawrence Livermore National Laboratory (USA).

**ESM** Earth System Modelling.

**Frontier** Frontier supercomputer at the Oak Ridge Leadership Computing Facility (USA).

**GPU** Graphics Processing Unit.

**HIP** Heterogeneous Interface for Portability, programming interface for AMD GPUs.

**HPC** High Performance Computing.

550    **JURECA-DC** Data Centric module of the Jülich Research on Exascale Cluster Architectures supercomputer at the Jülich Supercomputing Centre (Germany).

**JUWELS** Jülich Wizard for European Leadership Science, supercomputer at the Jülich Supercomputing Centre (Germany).

**JUWELS-booster** Booster module of the JUWELS supercomputer (Germany).

**Kokkos** Kokkos, a C++ performance portability layer.

555    **LUMI** LUMI supercomputer at CSC (Finland).

**MPI** Message Passing Interface for parallel computing.

**OpenMP** Open MultiProcessing, shared memory programming interface for parallel computing.

**SERGHEI** Simulation EnviRonment for Geomorphology, Hydrodynamics and Ecohydrology in Integrated form.

**SERGHEI-SWE** SERGHEI's shallow water equations solver.

560    **Summit** Summit supercomputer at the Oak Ridge Leadership Computing Facility (USA).

**SWE** Shallow Water Equations.

**SYCL** a programming model for hardware accelerators.

**UVM** Unified Virtual Memory.

**WSE** Water surface elevation.

# 565 References

Abderrezzak, K. E. K., Paquier, A., and Mignot, E.: Modelling flash flood propagation in urban areas using a two-dimensional numerical model, Natural Hazards, 50, 433–460, https://doi.org/10.1007/s11069-008-9300-0, 2008.

Alexander, F., Almgren, A., Bell, J., Bhattacharjee, A., Chen, J., Colella, P., Daniel, D., DeSlippe, J., Diachin, L., Draeger, E., Dubey, A., Dunning, T., Evans, T., Foster, I., Francois, M., Germann, T., Gordon, M., Habib, S., Halappanavar, M., Hamilton, S., Hart, W., Huang, 570 Z. H., Hungerford, A., Kasen, D., Kent, P. R. C., Kolev, T., Kothe, D. B., Kronfeld, A., Luo, Y., Mackenzie, P., McCallen, D., Messer, B., Mniszewski, S., Oehmen, C., Perazzo, A., Perez, D., Richards, D., Rider, W. J., Rieben, R., Roche, K., Siegel, A., Sprague, M., Steefel, C., Stevens, R., Syamlal, M., Taylor, M., Turner, J., Vay, J.-L., Voter, A. F., Windus, T. L., and Yelick, K.: Exascale applications: skin in the game, Philosophical Transactions of the Royal Society A: Mathematical, Physical and Engineering Sciences, 378, 20190 056, https://doi.org/10.1098/rsta.2019.0056, 2020.

575 An, H., Yu, S., Lee, G., and Kim, Y.: Analysis of an open source quadtree grid shallow water flow solver for flood simulation, Quaternary International, 384, 118–128, https://doi.org/http://dx.doi.org/10.1016/j.quaint.2015.01.032, 2015.

Arpaia, L. and Ricchiuto, M.: r-adaptation for Shallow Water flows: conservation, well balancedness, efficiency, Computers & Fluids, 160, 175–203, https://doi.org/10.1016/j.compfluid.2017.10.026, 2018.

Artigues, V., Kormann, K., Rampp, M., and Reuter, K.: Evaluation of performance portability frameworks for the implementation of a 580 particle-in-cell code, Concurrency and Computation Practice and Experience, 32, https://doi.org/10.1002/cpe.5640, 2019.

Aureli, F., Maranzoni, A., Mignosa, P., and Ziveri, C.: A weighted surface-depth gradient method for the numerical integration of the 2D shallow water equations with topography, Advances in Water Resources, 31, 962–974, https://doi.org/10.1016/j.advwatres.2008.03.005, 2008.

Aureli, F., Prost, F., Vacondio, R., Dazzi, S., and Ferrari, A.: A GPU-Accelerated Shallow-Water Scheme for Surface Runoff Simulations, 585 Water, 12, 637, https://doi.org/10.3390/w12030637, 2020.

Aureli, F., Maranzoni, A., and Petaccia, G.: Review of Historical Dam-Break Events and Laboratory Tests on Real Topography for the Validation of Numerical Models, Water, 13, 1968, https://doi.org/10.3390/w13141968, 2021.

Ayog, J. L., Kesserwani, G., Shaw, J., Sharifian, M. K., and Bau, D.: Second-order discontinuous Galerkin flood model: Comparison with industry-standard finite volume models, Journal of Hydrology, 594, 125 924, https://doi.org/10.1016/j.jhydrol.2020.125924, 2021.

590 Bates, P. and Roo, A. D.: A simple raster-based model for flood inundation simulation, Journal of Hydrology, 236, 54–77, https://doi.org/http://dx.doi.org/10.1016/S0022-1694(00)00278-X, 2000.

Bauer, P., Dueben, P. D., Hoefler, T., Quintino, T., Schulthess, T. C., and Wedi, N. P.: The digital revolution of Earth-system science, Nature Computational Science, 1, 104–113, https://doi.org/10.1038/s43588-021-00023-0, 2021.

Beckingsale, D. A., Burmark, J., Hornung, R., Jones, H., Killian, W., Kunen, A. J., Pearce, O., Robinson, P., Ryujin, B. S., and Scogland, 595 T. R.: RAJA: Portable Performance for Large-Scale Scientific Applications, in: 2019 IEEE/ACM International Workshop on Performance, Portability and Productivity in HPC (P3HPC), pp. 71–81, https://doi.org/10.1109/p3hpc49587.2019.00012, 2019.

Bellos, V. and Tsakiris, G.: A hybrid method for flood simulation in small catchments combining hydrodynamic and hydrological techniques, Journal of Hydrology, 540, 331–339, https://doi.org/10.1016/j.jhydrol.2016.06.040, 2016.

Berger, M. J., George, D. L., LeVeque, R. J., and Mandli, K. T.: The GeoClaw software for depth-averaged flows with adaptive refinement, 600 Advances in Water Resources, 34, 1195–1206, https://doi.org/10.1016/j.advwatres.2011.02.016, 2011.

Bertagna, L., Deakin, M., Guba, O., Sunderland, D., Bradley, A. M., Tezaur, I. K., Taylor, M. A., and Salinger, A. G.: HOMMEXX 1.0: a performance-portable atmospheric dynamical core for the Energy Exascale Earth System Model, Geoscientific Model Development, 12, 1423–1441, https://doi.org/10.5194/gmd-12-1423-2019, 2019.

605 Bomers, A., Schielen, R. M. J., and Hulscher, S. J. M. H.: The influence of grid shape and grid size on hydraulic river modelling performance, Environmental Fluid Mechanics, https://doi.org/10.1007/s10652-019-09670-4, 2019.

Bout, B. and Jetten, V.: The validity of flow approximations when simulating catchment-integrated flash floods, Journal of Hydrology, 556, 674–688, https://doi.org/10.1016/j.jhydrol.2017.11.033, 2018.

Bradford, S. F. and Sanders, B. F.: Finite-Volume Model for Shallow-Water Flooding of Arbitrary Topography, Journal of Hydraulic Engineering, 128, 289–298, https://doi.org/10.1061/(asce)0733-9429(2002)128:3(289), 2002.

610 Briggs, M. J., Synolakis, C. E., Harkins, G. S., and Green, D. R.: Laboratory experiments of tsunami runup on a circular island, Pure and Applied Geophysics PAGEOPH, 144, 569–593, https://doi.org/10.1007/bf00874384, 1995.

Brodtkorb, A. R., Sætra, M. L., and Altinakar, M.: Efficient shallow water simulations on GPUs: Implementation, visualization, verification, and validation, Computers & Fluids, 55, 1 – 12, https://doi.org/http://dx.doi.org/10.1016/j.compfluid.2011.10.012, 2012.

Brufau, P., García-Navarro, P., and Vázquez-Cendón, M. E.: Zero mass error using unsteady wetting-drying conditions in shallow flows over
615 dry irregular topography, International Journal for Numerical Methods in Fluids, 45, 1047–1082, https://doi.org/10.1002/fld.729, 2004.

Brunner, G.: HEC-RAS 2D User's Manual Version 6.0, Hydrologic Engineering Center, Davis, CA, USA, https://www.hec.usace.army.mil/confluence/rasdocs/r2dum/latest, 2021.

Brunner, P. and Simmons, C. T.: HydroGeoSphere: A Fully Integrated, Physically Based Hydrological Model, Ground Water, 50, 170–176, https://doi.org/10.1111/j.1745-6584.2011.00882.x, 2012.

620 Bruwier, M., Archambeau, P., Erpicum, S., Pirotton, M., and Dewals, B.: Discretization of the divergence formulation of the bed slope term in the shallow-water equations and consequences in terms of energy balance, Applied Mathematical Modelling, 40, 7532–7544, https://doi.org/10.1016/j.apm.2016.01.041, 2016.

Burguete, J., García-Navarro, P., and Murillo, J.: Friction term discretization and limitation to preserve stability and conservation in the 1D shallow-water model: Application to unsteady irrigation and river flow, International Journal for Numerical Methods in Fluids, 58,
625 403–425, https://doi.org/10.1002/fld.1727, 2008.

Buttinger-Kreuzhuber, A., Horváth, Z., Noelle, S., Blöschl, G., and Waser, J.: A fast second-order shallow water scheme on two-dimensional structured grids over abrupt topography, Advances in Water Resources, 127, 89–108, https://doi.org/10.1016/j.advwatres.2019.03.010, 2019.

Buttinger-Kreuzhuber, A., Konev, A., Horváth, Z., Cornel, D., Schwerdorf, I., Blöschl, G., and Waser, J.: An integrated GPU-accelerated
630 modeling framework for high-resolution simulations of rural and urban flash floods, Environmental Modelling & Software, p. 105480, https://doi.org/10.1016/j.envsoft.2022.105480, 2022.

Caldas Steinstraesser, J. G., Delenne, C., Finaud-Guyot, P., Guinot, V., Kahn Casapia, J. L., and Rousseau, A.: SW2D-LEMON: a new software for upscaled shallow water modeling, in: Simhydro 2021 - 6th International Conference Models for complex and global water issues - Practices and expectations, Sophia Antipolis, France, https://hal.inria.fr/hal-03224050, 2021.

635 Carlotto, T., Chaffe, P. L. B., dos Santos, C. I., and Lee, S.: SW2D-GPU: A two-dimensional shallow water model accelerated by GPGPU, Environmental Modelling & Software, p. 105205, https://doi.org/10.1016/j.envsoft.2021.105205, 2021.

Carroll, R. W. H., Bearup, L. A., Brown, W., Dong, W., Bill, M., and Willams, K. H.: Factors controlling seasonal groundwater and solute flux from snow-dominated basins, Hydrological Processes, 32, 2187–2202, https://doi.org/10.1002/hyp.13151, 2018.

Caviedes-Voullième, D. and Kesserwani, G.: Benchmarking a multiresolution discontinuous Galerkin shallow water model: Implications for computational hydraulics, Advances in Water Resources, 86, 14–31, https://doi.org/http://dx.doi.org/10.1016/j.advwatres.2015.09.016, 2015.

Caviedes-Voullième, D., García-Navarro, P., and Murillo, J.: Influence of mesh structure on 2D full shallow water equations and SCS Curve Number simulation of rainfall/runoff events, Journal of Hydrology, 448-449, 39 – 59, https://doi.org/https://doi.org/10.1016/j.jhydrol.2012.04.006, 2012.

Caviedes-Voullième, D., Fernández-Pato, J., and Hinz, C.: Cellular Automata and Finite Volume solvers converge for 2D shallow flow modelling for hydrological modelling, Journal of Hydrology, 563, 411–417, https://doi.org/10.1016/j.jhydrol.2018.06.021, 2018.

Caviedes-Voullième, D., Fernández-Pato, J., and Hinz, C.: Performance assessment of 2D Zero-Inertia and Shallow Water models for simulating rainfall-runoff processes, Journal of Hydrology, p. 124663, https://doi.org/10.1016/j.jhydrol.2020.124663, 2020a.

Caviedes-Voullième, D., Gerhard, N., Sikstel, A., and Müller, S.: Multiwavelet-based mesh adaptivity with Discontinuous Galerkin schemes: Exploring 2D shallow water problems, Advances in Water Resources, 138, 103 559, https://doi.org/10.1016/j.advwatres.2020.103559, 2020b.

Cea, L. and Bladé, E.: A simple and efficient unstructured finite volume scheme for solving the shallow water equations in overland flow applications, Water Resources Research, 51, 5464–5486, https://doi.org/10.1002/2014WR016547, 2015.

Cea, L., Garrido, M., and Puertas, J.: Experimental validation of two-dimensional depth-averaged models for forecasting rainfall–runoff from precipitation data in urban areas, Journal of Hydrology, 382, 88–102, https://doi.org/doi:10.1016/j.jhydrol.2009.12.020, 2010a.

Cea, L., Garrido, M., Puertas, J., Jácome, A., Río, H. D., and Suárez, J.: Overland flow computations in urban and industrial catchments from direct precipitation data using a two-dimensional shallow water model, Water Science and Technology, 62, 1998–2008, https://doi.org/10.2166/wst.2010.746, 2010b.

Chang, T.-J., Chang, Y.-S., and Chang, K.-H.: Modeling rainfall-runoff processes using smoothed particle hydrodynamics with mass-varied particles, Journal of Hydrology, 543, 749–758, https://doi.org/10.1016/j.jhydrol.2016.10.045, 2016.

Choi, B. H., Kim, D. C., Pelinovsky, E., and Woo, S. B.: Three-dimensional simulation of tsunami run-up around conical island, Coastal Engineering, 54, 618–629, https://doi.org/10.1016/j.coastaleng.2007.02.001, 2007.

Clark, M. P., Bierkens, M. F. P., Samaniego, L., Woods, R. A., Uijlenhoet, R., Bennett, K. E., Pauwels, V. R. N., Cai, X., Wood, A. W., and Peters-Lidard, C. D.: The evolution of process-based hydrologic models: historical challenges and the collective quest for physical realism, Hydrology and Earth System Sciences, 21, 3427–3440, https://doi.org/10.5194/hess-21-3427-2017, 2017.

Coon, E., Svyatsky, D., Jan, A., Kikinzon, E., Berndt, M., Atchley, A., Harp, D., Manzini, G., Shelef, E., Lipnikov, K., Garimella, R., Xu, C., Moulton, D., Karra, S., Painter, S., Jafarov, E., and Molins, S.: Advanced Terrestrial Simulator, https://doi.org/10.11578/DC.20190911.1, 2019.

Costabile, P. and Costanzo, C.: A 2D SWEs framework for efficient catchment-scale simulations: hydrodynamic scaling properties of river networks and implications for non-uniform grids generation, Journal of Hydrology, p. 126306, https://doi.org/10.1016/j.jhydrol.2021.126306, 2021.

Costabile, P., Costanzo, C., Ferraro, D., and Barca, P.: Is HEC-RAS 2D accurate enough for storm-event hazard assessment? Lessons learnt from a benchmarking study based on rain-on-grid modelling, Journal of Hydrology, 603, 126 962, https://doi.org/10.1016/j.jhydrol.2021.126962, 2021.

Crompton, O., Katul, G. G., and Thompson, S.: Resistance formulations in shallow overland flow along a hillslope covered with patchy vegetation, Water Resources Research, 56, e2020WR027 194, 2020.

David, A. and Schmalz, B.: A Systematic Analysis of the Interaction between Rain-on-Grid-Simulations and Spatial Resolution in 2D Hydrodynamic Modeling, Water, 13, 2346, https://doi.org/10.3390/w13172346, 2021.

Dazzi, S., Vacondio, R., Palù, A. D., and Mignosa, P.: A local time stepping algorithm for GPU-accelerated 2D shallow water models, Advances in Water Resources, 111, 274–288, https://doi.org/10.1016/j.advwatres.2017.11.023, 2018.

Delestre, O., Lucas, C., Ksinant, P., Darboux, F., Laguerre, C., Vo, T., James, F., and Cordier, S.: SWASHES: a compilation of shallow water analytic solutions for hydraulic and environmental studies, International Journal for Numerical Methods in Fluids, 72, 269–300, https://doi.org/10.1002/fld.3741, 2013.

Delestre, O., Darboux, F., James, F., Lucas, C., Laguerre, C., and Cordier, S.: FullSWOF: Full Shallow-Water equations for Overland Flow, The Journal of Open Source Software, 2, 448, https://doi.org/10.21105/joss.00448, 2017.

Demeshko, I., Watkins, J., Tezaur, I. K., Guba, O., Spotz, W. F., Salinger, A. G., Pawlowski, R. P., and Heroux, M. A.: Toward performance portability of the Albany finite element analysis code using the Kokkos library, The International Journal of High Performance Computing Applications, 33, 332–352, https://doi.org/10.1177/1094342017749957, 2018.

Djemame, K. and Carr, H.: Exascale Computing Deployment Challenges, in: Economics of Grids, Clouds, Systems, and Services, pp. 211–216, Springer International Publishing, https://doi.org/10.1007/978-3-030-63058-4_19, 2020.

Dullo, T. T., Darkwah, G. K., Gangrade, S., Morales-Hernández, M., Sharif, M. B., Kalyanapu, A. J., Kao, S.-C., Ghafoor, S., and Ashfaq, M.: Assessing climate-change-induced flood risk in the Conasauga River watershed: an application of ensemble hydrodynamic inundation modeling, Natural Hazards and Earth System Sciences, 21, 1739–1757, https://doi.org/10.5194/nhess-21-1739-2021, 2021a.

Dullo, T. T., Gangrade, S., Morales-Hernández, M., Sharif, M. B., Kao, S.-C., Kalyanapu, A. J., Ghafoor, S., and Evans, K. J.: Simulation of Hurricane Harvey flood event through coupled hydrologic-hydraulic models: Challenges and next steps, Journal of Flood Risk Management, https://doi.org/10.1111/jfr3.12716, 2021b.

Duran, A., Liang, Q., and Marche, F.: On the well-balanced numerical discretization of shallow water equations on unstructured meshes, Journal of Computational Physics, 235, 565 – 586, https://doi.org/http://dx.doi.org/10.1016/j.jcp.2012.10.033, 2013.

Echeverribar, I., Morales-Hernández, M., Brufau, P., and García-Navarro, P.: 2D numerical simulation of unsteady flows for large scale floods prediction in real time, Advances in Water Resources, 134, 103 444, https://doi.org/10.1016/j.advwatres.2019.103444, 2019.

Echeverribar, I., Morales-Hernández, M., Brufau, P., and García-Navarro, P.: Analysis of the performance of a hybrid CPU/GPU 1D2D coupled model for real flood cases, Journal of Hydroinformatics, 22, 1198–1216, https://doi.org/10.2166/hydro.2020.032, 2020.

Edwards, H. C., Trott, C. R., and Sunderland, D.: Kokkos: Enabling manycore performance portability through polymorphic memory access patterns, Journal of Parallel and Distributed Computing, 74, 3202 – 3216, https://doi.org/https://doi.org/10.1016/j.jpdc.2014.07.003, domain-Specific Languages and High-Level Frameworks for High-Performance Computing, 2014.

Fan, Y., Clark, M., Lawrence, D. M., Swenson, S., Band, L. E., Brantley, S. L., Brooks, P. D., Dietrich, W. E., Flores, A., Grant, G., Kirchner, J. W., Mackay, D. S., McDonnell, J. J., Milly, P. C. D., Sullivan, P. L., Tague, C., Ajami, H., Chaney, N., Hartmann, A., Hazenberg, P., McNamara, J., Pelletier, J., Perket, J., Rouholahnejad-Freund, E., Wagener, T., Zeng, X., Beighley, E., Buzan, J., Huang, M., Livneh, B., Mohanty, B. P., Nijssen, B., Safeeq, M., Shen, C., van Verseveld, W., Volk, J., and Yamazaki, D.: Hillslope Hydrology in Global Change Research and Earth System Modeling, Water Resources Research, https://doi.org/10.1029/2018wr023903, 2019.

Fatichi, S., Vivoni, E. R., Ogden, F. L., Ivanov, V. Y., Mirus, B., Gochis, D., Downer, C. W., Camporese, M., Davison, J. H., Ebel, B., Jones, N., Kim, J., Mascaro, G., Niswonger, R., Restrepo, P., Rigon, R., Shen, C., Sulis, M., and Tarboton, D.: An overview of current applications, challenges, and future trends in distributed process-based models in hydrology, Journal of Hydrology, 537, 45 – 60, https://doi.org/http://dx.doi.org/10.1016/j.jhydrol.2016.03.026, 2016.

715 Fernández-Pato, J. and García-Navarro, P.: A 2D zero-inertia model for the solution of overland flow problems in flexible meshes, Journal of Hydrologic Engineering - ASCE, 2016.

Fernández-Pato, J., Caviedes-Voullième, D., and García-Navarro, P.: Rainfall/runoff simulation with 2D full shallow water equations: sensitivity analysis and calibration of infiltration parameters, Journal of Hydrology, 536, 496–513, https://doi.org/http://dx.doi.org/10.1016/j.jhydrol.2016.03.021, 2016.

720 Fernández-Pato, J., Martínez-Aranda, S., and García-Navarro, P.: A 2D finite volume simulation tool to enable the assessment of combined hydrological and morphodynamical processes in mountain catchments, Advances in Water Resources, 141, 103 617, https://doi.org/10.1016/j.advwatres.2020.103617, 2020.

Gan, L., Fu, H., and Yang, G.: Translating novel HPC techniques into efficient geoscience solutions, Journal of Computational Science, p. 101212, https://doi.org/10.1016/j.jocs.2020.101212, 2020.

725 García-Alén, G., González-Cao, J., Fernández-Nóvoa, D., Gómez-Gesteira, M., Cea, L., and Puertas, J.: Analysis of two sources of variability of basin outflow hydrographs computed with the 2D shallow water model Iber: Digital Terrain Model and unstructured mesh size, Journal of Hydrology, 612, 128 182, https://doi.org/10.1016/j.jhydrol.2022.128182, 2022.

García-Feal, O., González-Cao, J., Gómez-Gesteira, M., Cea, L., Domínguez, J., and Formella, A.: An Accelerated Tool for Flood Modelling Based on Iber, Water, 10, 1459, https://doi.org/10.3390/w10101459, 2018.

730 García-Navarro, P., Murillo, J., Fernández-Pato, J., Echeverribar, I., and Morales-Hernández, M.: The shallow water equations and their application to realistic cases, Environmental Fluid Mechanics, https://doi.org/10.1007/s10652-018-09657-7, 2019.

George, D. L.: Adaptive finite volume methods with well-balanced Riemann solvers for modeling floods in rugged terrain: Application to the Malpasset dam-break flood (France, 1959), International Journal for Numerical Methods in Fluids, 66, 1000–1018, https://doi.org/10.1002/fld.2298, 2010.

735 Giardino, J. R. and Houser, C.: Introduction to the critical zone, in: Developments in Earth Surface Processes, edited by J. R. Giardino, C. H., vol. 19, chap. 1, Elsevier B.V., Amsterdam, the Netherlands, 2015.

Ginting, B. M.: Central-upwind scheme for 2D turbulent shallow flows using high-resolution meshes with scalable wall functions, Computers & Fluids, 179, 394–421, https://doi.org/10.1016/j.compfluid.2018.11.014, 2019.

Gottardi, G. and Venutelli, M.: An accurate time integration method for simplified overland flow models, Advances in Water Resources, 31,
740 173–180, https://doi.org/http://dx.doi.org/10.1016/j.advwatres.2007.08.004, 2008.

Govindaraju, R. S., Kavvas, M. L., and Jones, S. E.: Approximate Analytical Solutions for Overland Flows, Water Resources Research, 26, 2903–2912, https://doi.org/10.1029/WR026i012p02903, 1990.

Grant, R. and the Ecosys development team: The Ecosys Modelling Project, https://ecosys.ualberta.ca/, 2022.

Grant, R. F., Barr, A. G., Black, T. A., Gaumont-Guay, D., Iwashita, H., Kidson, J., McCaughey, H., Morgenstern, K., Murayama, S., Nesic,
745 Z., Saigusa, N., Shashkov, A., and Zha, T.: Net ecosystem productivity of boreal jack pine stands regenerating from clearcutting under current and future climates, Global Change Biology, 13, 1423–1440, https://doi.org/10.1111/j.1365-2486.2007.01363.x, 2007.

Grete, P., Glines, F. W., and O'Shea, B. W.: K-Athena: A Performance Portable Structured Grid Finite Volume Magnetohydrodynamics Code, IEEE TRANSACTIONS ON PARALLEL AND DISTRIBUTED SYSTEMS, 32, 85–97, https://doi.org/10.1109/tpds.2020.3010016, 2021.

750 Halver, R., Meinke, J. H., and Sutmann, G.: Kokkos implementation of an Ewald Coulomb solver and analysis of performance portability, Journal of Parallel and Distributed Computing, 138, 48–54, https://doi.org/10.1016/j.jpdc.2019.12.003, 2020.

Hartanto, I., Beevers, L., Popescu, I., and Wright, N.: Application of a coastal modelling code in fluvial environments, Environmental Modelling & Software, 26, 1685–1695, https://doi.org/10.1016/j.envsoft.2011.05.014, 2011.

Hervouet, J.-M. and Petitjean, A.: Malpasset dam-break revisited with two-dimensional computations, Journal of Hydraulic Research, 37, 755    777–788, https://doi.org/10.1080/00221689909498511, 1999.

Hiver, J.: Adverse-Slope and Slope (bump), in: Concerted Action on Dam Break Modelling: Objectives, Project Report, Test Cases, Meeting Proceedings, edited by Soares-Frazão, S., Morris, M., and Zech, Y., vol. CD-ROM, Université Catholique de Louvain, Civil Engineering Department, Hydraulics Division, Louvain-la-Neuve, Belgium, 2000.

Hou, J., Liang, Q., Simons, F., and Hinkelmann, R.: A stable 2D unstructured shallow flow model for simulations of wetting and drying over 760    rough terrains, Computers & Fluids, 82, 132 – 147, https://doi.org/http://dx.doi.org/10.1016/j.compfluid.2013.04.015, 2013a.

Hou, J., Simons, F., Mahgoub, M., and Hinkelmann, R.: A robust well-balanced model on unstructured grids for shallow water flows with wetting and drying over complex topography, Computer Methods in Applied Mechanics and Engineering, 257, 126 – 149, https://doi.org/http://dx.doi.org/10.1016/j.cma.2013.01.015, 2013b.

Hou, J., Liang, Q., Zhang, H., and Hinkelmann, R.: An efficient unstructured MUSCL scheme for solving the 2D shallow water equations, 765    Environmental Modelling & Software, 66, 131–152, https://doi.org/10.1016/j.envsoft.2014.12.007, 2015.

Hou, J., Wang, R., Liang, Q., Li, Z., Huang, M. S., and Hinkelmann, R.: Efficient surface water flow simulation on static Cartesian grid with local refinement according to key topographic features, Computers & Fluids, 176, 117–134, https://doi.org/10.1016/j.compfluid.2018.03.024, 2018.

Hou, J., Kang, Y., Hu, C., Tong, Y., Pan, B., and Xia, J.: A GPU-based numerical model coupling hydrodynamical and morphological 770    processes, International Journal of Sediment Research, 35, 386–394, https://doi.org/10.1016/j.ijsrc.2020.02.005, 2020.

Hubbard, S. S., Williams, K. H., Agarwal, D., Banfield, J., Beller, H., Bouskill, N., Brodie, E., Carroll, R., Dafflon, B., Dwivedi, D., Falco, N., Faybishenko, B., Maxwell, R., Nico, P., Steefel, C., Steltzer, H., Tokunaga, T., Tran, P. A., Wainwright, H., and Varadharajan, C.: The East River, Colorado, Watershed: A Mountainous Community Testbed for Improving Predictive Understanding of Multiscale Hydrological-Biogeochemical Dynamics, Vadose Zone Journal, 17, 180 061, https://doi.org/10.2136/vzj2018.03.0061, 2018.

775 Jain, M. K. and Kothyari, U. C.: A GIS based distributed rainfall-runoff model, Journal of Hydrology, 299, 107–135, 2004.

Jeong, W., Yoon, J.-S., and Cho, Y.-S.: Numerical study on effects of building groups on dam-break flow in urban areas, Journal of Hydro-environment Research, 6, 91–99, https://doi.org/10.1016/j.jher.2012.01.001, 2012.

Jodhani, K. H., Patel, D., and Madhavan, N.: A review on analysis of flood modelling using different numerical models, Materials Today: Proceedings, https://doi.org/10.1016/j.matpr.2021.07.405, 2021.

780 Kesserwani, G. and Liang, Q.: Well-balanced RKDG2 solutions to the shallow water equations over irregular domains with wetting and drying, Computers & Fluids, 39, 2040–2050, https://doi.org/10.1016/j.compfluid.2010.07.008, 2010.

Kesserwani, G. and Liang, Q.: Dynamically adaptive grid based discontinuous Galerkin shallow water model, Advances In Water Resources, 37, 23–39, https://doi.org/10.1016/j.advwatres.2011.11.006, 2012.

Kesserwani, G. and Sharifian, M. K.: (Multi)wavelets increase both accuracy and efficiency of standard Godunov-type hydrodynamic models: 785    Robust 2D approaches, Advances in Water Resources, 144, 103 693, https://doi.org/10.1016/j.advwatres.2020.103693, 2020.

Kesserwani, G. and Sharifian, M. K.: (Multi)wavelet-based Godunov-type simulators of flood inundation: static versus dynamic adaptivity, Advances in Water Resources, p. 104357, https://doi.org/10.1016/j.advwatres.2022.104357, 2022.

Kesserwani, G., Shaw, J., Sharifian, M. K., Bau, D., Keylock, C. J., Bates, P. D., and Ryan, J. K.: (Multi)wavelets increase both accuracy and efficiency of standard Godunov-type hydrodynamic models, Advances in Water Resources, 129, 31–55, https://doi.org/10.1016/j.advwatres.2019.04.019, 2019.

Kim, B., Sanders, B. F., Schubert, J. E., and Famiglietti, J. S.: Mesh type tradeoffs in 2D hydrodynamic modeling of flooding with a Godunov-based flow solver, Advances in Water Resources, 68, 42 – 61, https://doi.org/http://dx.doi.org/10.1016/j.advwatres.2014.02.013, 2014.

Kirstetter, G., Delestre, O., Lagrée, P.-Y., Popinet, S., and Josserand, C.: B-flood 1.0: an open-source Saint-Venant model for flash flood simulation using adaptive refinement, Geoscientific Model Development, https://doi.org/10.5194/gmd-2021-15, 2021.

Kobayashi, K., Kitamura, D., Ando, K., and Ohi, N.: Parallel computing for high-resolution/large-scale flood simulation using the K super-computer, Hydrological Research Letters, 9, 61–68, https://doi.org/10.3178/hrl.9.61, 2015.

Kollet, S., Sulis, M., Maxwell, R. M., Paniconi, C., Putti, M., Bertoldi, G., Coon, E. T., Cordano, E., Endrizzi, S., Kikinzon, E., Mouche, E., Mügler, C., Park, Y.-J., Refsgaard, J. C., Stisen, S., and Sudicky, E.: The integrated hydrologic model intercomparison project, IH-MIP2: A second set of benchmark results to diagnose integrated hydrology and feedbacks, Water Resources Research, 53, 867–890, https://doi.org/10.1002/2016wr019191, 2017.

Kuffour, B. N. O., Engdahl, N. B., Woodward, C. S., Condon, L. E., Kollet, S., and Maxwell, R. M.: Simulating coupled surface–subsurface flows with ParFlow v3.5.0: capabilities, applications, and ongoing development of an open-source, massively parallel, integrated hydrologic model, Geoscientific Model Development, 13, 1373–1397, https://doi.org/10.5194/gmd-13-1373-2020, 2020.

Lacasta, A., Morales-Hernández, M., Murillo, J., and García-Navarro, P.: An optimized GPU implementation of a 2D free surface simulation model on unstructured meshes, Advances in Engineering Software, 78, 1 – 15, https://doi.org/http://dx.doi.org/10.1016/j.advengsoft.2014.08.007, 2014.

Lacasta, A., Morales-Hernández, M., Murillo, J., and García-Navarro, P.: GPU implementation of the 2D shallow water equations for the simulation of rainfall/runoff events, Environ Earth Sci, 74, 7295–7305, https://doi.org/10.1007/s12665-015-4215-z, 2015.

Lawrence, B. N., Rezny, M., Budich, R., Bauer, P., Behrens, J., Carter, M., Deconinck, W., Ford, R., Maynard, C., Mullerworth, S., Osuna, C., Porter, A., Serradell, K., Valcke, S., Wedi, N., and Wilson, S.: Crossing the chasm: how to develop weather and climate models for next generation computers?, Geoscientific Model Development, 11, 1799–1821, https://doi.org/10.5194/gmd-11-1799-2018, 2018.

Leiserson, C. E., Thompson, N. C., Emer, J. S., Kuszmaul, B. C., Lampson, B. W., Sanchez, D., and Schardl, T. B.: There's plenty of room at the Top: What will drive computer performance after Moore's law?, Science, 368, https://doi.org/10.1126/science.aam9744, 2020.

Li, Z., Özgen-Xian, I., and Maina, F. Z.: A mass-conservative predictor-corrector solution to the 1D Richards equation with adaptive time control, Journal of Hydrology, 592, 125 809, https://doi.org/10.1016/j.jhydrol.2020.125809, 2021.

Liang, D., Lin, B., and Falconer, R. A.: A boundary-fitted numerical model for flood routing with shock-capturing capability, Journal of Hydrology, 332, 477–486, https://doi.org/doi:10.1016/j.jhydrol.2006.08.002, 2007.

Liang, Q., Hou, J., and Xia, X.: Contradiction between the C-property and mass conservation in adaptive grid based shallow flow models: cause and solution, International Journal for Numerical Methods in Fluids, 78, 17–36, https://doi.org/10.1002/fld.4005, 2015.

Liang, Q., Smith, L., and Xia, X.: New prospects for computational hydraulics by leveraging high-performance heterogeneous computing techniques, Journal of Hydrodynamics, Ser. B, 28, 977 – 985, https://doi.org/http://dx.doi.org/10.1016/S1001-6058(16)60699-6, 2016.

Lichtner, P. C., Hammond, G. E., Lu, C., Karra, S., Bisht, G., Andre, B., Mills, R., and Kumar, J.: PFLOTRAN user manual: A massively parallel reactive flow and transport model for describing surface and subsurface processes, Tech. rep., Los Alamos National Laboratory, New Mexico, USA, 2015.

Liu, P. L. F., Cho, Y.-S., Briggs, M. J., Kanoglu, U., and Synolakis, C. E.: Runup of solitary waves on a circular Island, Journal of Fluid Mechanics, 302, 259–285, https://doi.org/10.1017/s0022112095004095, 1995.

Loukili, Y. and Soulaïmani, A.: Numerical Tracking of Shallow Water Waves by the Unstructured Finite Volume WAF Approximation, International Journal for Computational Methods in Engineering Science and Mechanics, 8, 75–88, https://doi.org/10.1080/15502280601149577, 2007.

Lynett, P. J., Wu, T.-R., and Liu, P. L.-F.: Modeling wave runup with depth-integrated equations, Coastal Engineering, 46, 89–107, https://doi.org/10.1016/s0378-3839(02)00043-1, 2002.

MacDonald, I., Baines, M., Nichols, N., and PG, S.: Comparison of some Steady StateSaint-Venant Solvers forsome Test Problems withAnalytic Solutions, Tech. rep., University of Reading, 1995.

Maneta, M. P. and Silverman, N. L.: A spatially distributed model to simulate water, energy, and vegetation dynamics using information from regional climate models, Earth Interactions, 17, 11.1–11.44, 2013.

Mann, A.: Core Concept: Nascent exascale supercomputers offer promise, present challenges, Proceedings of the National Academy of Sciences, 117, 22 623–22 625, https://doi.org/10.1073/pnas.2015968117, 2020.

Martínez-Aranda, S., Fernández-Pato, J., Caviedes-Voullième, D., García-Palacín, I., and García-Navarro, P.: Towards transient experimental water surfaces: A new benchmark dataset for 2D shallow water solvers, Advances in Water Resources, 121, 130–149, https://doi.org/10.1016/j.advwatres.2018.08.013, 2018.

Matsuyama, M. and Tanaka, H.: An experimental study oh the highest run-up height in the 1993 Hokkaido Nansei-oki earthquake tsunami, ITS Proceedings, pp. 879–889, 2001.

Morales-Hernández, M., García-Navarro, P., and Murillo, J.: A large time step 1D upwind explicit scheme (CFL>1): Application to shallow water equations, Journal of Computational Physics, 231, 6532 – 6557, https://doi.org/http://dx.doi.org/10.1016/j.jcp.2012.06.017, 2012.

Morales-Hernández, M., Hubbard, M., and García-Navarro, P.: A 2D extension of a Large Time Step explicit scheme (CFL>1) for unsteady problems with wet/dry boundaries, Journal of Computational Physics, 263, 303 – 327, https://doi.org/http://dx.doi.org/10.1016/j.jcp.2014.01.019, 2014.

Morales-Hernández, M., Sharif, M. B., Gangrade, S., Dullo, T. T., Kao, S.-C., Kalyanapu, A., Ghafoor, S. K., Evans, K. J., Madadi-Kandjani, E., and Hodges, B. R.: High-performance computing in water resources hydrodynamics, Journal of Hydroinformatics, https://doi.org/10.2166/hydro.2020.163, 2020.

Morales-Hernández, M., Sharif, M. B., Kalyanapu, A., Ghafoor, S., Dullo, T., Gangrade, S., Kao, S.-C., Norman, M., and Evans, K.: TRITON: A Multi-GPU open source 2D hydrodynamic flood model, Environmental Modelling & Software, 141, 105 034, https://doi.org/10.1016/j.envsoft.2021.105034, 2021.

Moulinec, C., Denis, C., Pham, C.-T., Rougé, D., Hervouet, J.-M., Razafindrakoto, E., Barber, R., Emerson, D., and Gu, X.-J.: TELEMAC: An efficient hydrodynamics suite for massively parallel architectures, Computers & Fluids, 51, 30–34, https://doi.org/10.1016/j.compfluid.2011.07.003, 2011.

Mügler, C., Planchon, O., Patin, J., Weill, S., Silvera, N., Richard, P., and Mouche, E.: Comparison of roughness models to simulate overland flow and tracer transport experiments under simulated rainfall at plot scale, Journal of Hydrology, 402, 25–40, https://doi.org/http://dx.doi.org/10.1016/j.jhydrol.2011.02.032, 2011.

Murillo, J. and García-Navarro, P.: Weak solutions for partial differential equations with source terms: Application to the shallow water equations, Journal of Computational Physics, 229, 4327–4368, https://doi.org/10.1016/j.jcp.2010.02.016, 2010.

Murillo, J. and García-Navarro, P.: Augmented versions of the HLL and HLLC Riemann solvers including source terms in one and two dimensions for shallow flow applications, Journal of Computational Physics, 231, 6861–6906, https://doi.org/10.1016/j.jcp.2012.06.031, 2012.

Murillo, J., García-Navarro, P., and Burguete, J.: Time step restrictions for well-balanced shallow water solutions in non-zero velocity steady states, International Journal for Numerical Methods in Fluids, 60, 1351–1377, https://doi.org/10.1002/fld.1939, 2009.

Navas-Montilla, A. and Murillo, J.: 2D well-balanced augmented ADER schemes for the Shallow Water Equations with bed elevation and extension to the rotating frame, Journal of Computational Physics, 372, 316–348, https://doi.org/10.1016/j.jcp.2018.06.039, 2018.

Nikolos, I. and Delis, A.: An unstructured node-centered finite volume scheme for shallow water flows with wet/dry fronts over complex topography, Computer Methods in Applied Mechanics and Engineering, 198, 3723 – 3750, https://doi.org/http://dx.doi.org/10.1016/j.cma.2009.08.006, 2009.

Özgen, I., Liang, D., and Hinkelmann, R.: Shallow water equations with depth-dependent anisotropic porosity for subgrid-scale topography, Applied Mathematical Modelling, https://doi.org/http://dx.doi.org/10.1016/j.apm.2015.12.012, 2015a.

Özgen, I., Teuber, K., Simons, F., Liang, D., and Hinkelmann, R.: Upscaling the shallow water model with a novel roughness formulation, Environ Earth Sci, 74, 7371–7386, https://doi.org/10.1007/s12665-015-4726-7, 2015b.

Özgen-Xian, I., Kesserwani, G., Caviedes-Voullième, D., Molins, S., Xu, Z., Dwivedi, D., Moulton, J. D., and Steefel, C. I.: Wavelet-based local mesh refinement for rainfall–runoff simulations, Journal of Hydroinformatics, https://doi.org/10.2166/hydro.2020.198, 2020.

Özgen-Xian, I., Xia, X., Liang, Q., Hinkelmann, R., Liang, D., and Hou, J.: Innovations Towards the Next Generation of Shallow Flow Models, Advances in Water Resources, p. 103867, https://doi.org/10.1016/j.advwatres.2021.103867, 2021.

Paniconi, C. and Putti, M.: Physically based modeling in catchment hydrology at 50: Survey and outlook, Water Resources Research, 51, 7090–7129, https://doi.org/10.1002/2015WR017780, 2015.

Park, Kim, and Kim: 2D GPU-Accelerated High Resolution Numerical Scheme for Solving Diffusive Wave Equations, Water, 11, 1447, https://doi.org/10.3390/w11071447, 2019.

Petaccia, G., Soares-Frazão, S., Savi, F., Natale, L., and Zech, Y.: Simplified versus Detailed Two-Dimensional Approaches to Transient Flow Modeling in Urban Areas, Journal of Hydraulic Engineering, 136, 262–266, https://doi.org/10.1061/(asce)hy.1943-7900.0000154, 2010.

Roe, P.: Approximate Riemann solvers, parameter vectors, and difference schemes, Journal of Computational Physics, 43, 357–372, https://doi.org/10.1016/0021-9991(81)90128-5, 1981.

Schulthess, T. C.: Programming revisited, Nature Physics, 11, 369–373, https://doi.org/10.1038/nphys3294, 2015.

Schwanenberg, D. and Harms, M.: Discontinuous Galerkin Finite-Element Method for Transcritical Two-Dimensional Shallow Water Flows, Journal of Hydraulic Engineering, 130, 412–421, https://doi.org/http://dx.doi.org/10.1061/(ASCE)0733-9429(2004)130:5(412), 2004.

Serrano-Pacheco, A., Murillo, J., and Garcia-Navarro, P.: A finite volume method for the simulation of the waves generated by landslides, Journal of Hydrology, 373, 273–289, https://doi.org/10.1016/j.jhydrol.2009.05.003, 2009.

Sharif, M. B., Ghafoor, S. K., Hines, T. M., Morales-Hernändez, M., Evans, K. J., Kao, S.-C., Kalyanapu, A. J., Dullo, T. T., and Gangrade, S.: Performance Evaluation of a Two-Dimensional Flood Model on Heterogeneous High-Performance Computing Architectures, in: Proceedings of the Platform for Advanced Scientific Computing Conference, ACM, https://doi.org/10.1145/3394277.3401852, 2020.

Shaw, J., Kesserwani, G., Neal, J., Bates, P., and Sharifian, M. K.: LISFLOOD-FP 8.0: the new discontinuous Galerkin shallow water solver for multi-core CPUs and GPUs, Geoscientific Model Development, https://doi.org/10.5194/gmd-2020-340, 2020.

37

900    Simons, F., Busse, T., Hou, J., Özgen, I., and Hinkelmann, R.: A model for overland flow and associated processes within the Hydroinformatics Modelling System, Journal of Hydroinformatics, 16, 375–391, https://doi.org/10.2166/hydro.2013.173, 2014.

Singh, J., Altinakar, M. S., and Ding, Y.: Numerical Modeling of Rainfall-Generated Overland Flow Using Nonlinear Shallow-Water Equations, Journal of Hydrologic Engineering, 20, 04014 089, https://doi.org/http://dx.doi.org/10.1061/(ASCE)HE.1943-5584.0001124, 2015.

Sivapalan, M.: From engineering hydrology to Earth system science: milestones in the transformation of hydrologic science, Hydrology and
905    Earth System Sciences, 22, 1665–1693, https://doi.org/10.5194/hess-22-1665-2018, 2018.

Sætra, M. L., Brodtkorb, A. R., and Lie, K.-A.: Efficient GPU-Implementation of Adaptive Mesh Refinement for the Shallow-Water Equations, Journal of Scientific Computing, 63, 23–48, https://doi.org/10.1007/s10915-014-9883-4, 2015.

Smith, L. S. and Liang, Q.: Towards a generalised GPU/CPU shallow-flow modelling tool, Computers & Fluids, 88, 334 – 343, https://doi.org/http://dx.doi.org/10.1016/j.compfluid.2013.09.018, 2013.

910    Soares-Frazão, S.: Experiments of dam-break wave over a triangular bottom sill, Journal of Hydraulic Research, 45, 19–26, https://doi.org/10.1080/00221686.2007.9521829, 2007.

Soares-Frazão, S. and Zech, Y.: Dam-break flow through an idealised city, Journal of Hydraulic Research, 46, 648–658, https://doi.org/10.3826/jhr.2008.3164, 2008.

Steefel, C. I.: CrunchFlow: Software for modeling multicomponent reactive flow and transport, Tech. rep., Lawrence Berkeley National
915    Laboratory, California, USA, 2009.

Steffen, L., Amann, F., and Hinkelmann, R.: Concepts for performance improvements of shallow water flow simulations, in: Proceedings of the 1st IAHR Young Professionals Congress, online, 2020.

Stoker, J.: Water Waves: The Mathematical Theory with Applications, New York Interscience Publishers. Wiley, 1957.

Su, B., Huang, H., and Zhu, W.: An urban pluvial flood simulation model based on diffusive wave approximation of shallow water equations,
920    Hydrology Research, 50, 138–154, https://doi.org/10.2166/nh.2017.233, 2017.

Suarez, E., Eicker, N., and Lippert, T.: Modular Supercomputing Architecture: From Idea to Production, in: Contemporary High Performance Computing, pp. 223–255, CRC Press, https://doi.org/10.1201/9781351036863-9, 2019.

Tatard, L., Planchon, O., Wainwright, J., Nord, G., Favis-Mortlock, D., Silvera, N., Ribolzi, O., Esteves, M., and Huang, C. H.: Measurement and modelling of high-resolution flow-velocity data under simulated rainfall on a low-slope sandy soil, Journal of Hydrology, 348, 1–12,
925    https://doi.org/http://dx.doi.org/10.1016/j.jhydrol.2007.07.016, 2008.

Thacker, W.: Some exact solutions to the nonlinear shallow-water wave equations, Journal of Fluid Mechanics, 107, 499–508, https://doi.org/doi:10.1017/S0022112081001882, 1981.

The third international workshop on long-wave runup models: http://isec.nacse.org/workshop/2004_cornell/bmark2.html, 2004.

Toro, E.: Shock-Capturing Methods for Free-Surface Shallow Flows, Wiley, 2001.

930    Trott, C., Berger-Vergiat, L., Poliakoff, D., Rajamanickam, S., Lebrun-Grandie, D., Madsen, J., Awar, N. A., Gligoric, M., Shipman, G., and Womeldorff, G.: The Kokkos EcoSystem: Comprehensive Performance Portability for High Performance Computing, Computing in Science & Engineering, 23, 10–18, https://doi.org/10.1109/mcse.2021.3098509, 2021.

Turchetto, M., Palu, A. D., and Vacondio, R.: A general design for a scalable MPI-GPU multi-resolution 2D numerical solver, IEEE Transactions on Parallel and Distributed Systems, pp. 1–1, https://doi.org/10.1109/tpds.2019.2961909, 2019.

935    Vacondio, R., Palù, A. D., and Mignosa, P.: GPU-enhanced Finite Volume Shallow Water solver for fast flood simulations, Environmental Modelling & Software, 57, 60–75, https://doi.org/10.1016/j.envsoft.2014.02.003, 2014.

Vacondio, R., Palù, A. D., Ferrari, A., Mignosa, P., Aureli, F., and Dazzi, S.: A non-uniform efficient grid type for GPU-parallel Shallow Water Equations models, Environmental Modelling & Software, 88, 119–137, https://doi.org/10.1016/j.envsoft.2016.11.012, 2017.

Valiani, A., Caleffi, V., and Zanni, A.: Case Study: Malpasset Dam-Break Simulation using a Two-Dimensional Finite Volume Method,
940      Journal of Hydraulic Engineering, 128, 460–472, https://doi.org/http://dx.doi.org/10.1061/(ASCE)0733-9429(2002)128:5(460), 2002.

Vanderbauwhede, W.: Making legacy Fortran code type safe through automated program transformation, The Journal of Supercomputing, 78, 2988–3028, 2021.

Vanderbauwhede, W. and Davidson, G.: Domain-specific acceleration and auto-parallelization of legacy scientific code in FORTRAN 77 using source-to-source compilation, Computers and Fluids, 173, 1–5, 2018.

945 Vanderbauwhede, W. and Takemi, T.: An investigation into the feasibility and benefits of GPU/multicore acceleration of the weather research and forecasting model, in: 2013 International Conference on High Performance Computing and Simulation (HPCS), Helsinki, Finland, 2013.

Vater, S., Beisiegel, N., and Behrens, J.: A limiter-based well-balanced discontinuous Galerkin method for shallow-water flows with wetting and drying: Triangular grids, International Journal for Numerical Methods in Fluids, https://doi.org/10.1002/fld.4762, 2019.

950 Wang, Y., Liang, Q., Kesserwani, G., and Hall, J. W.: A 2D shallow flow model for practical dam-break simulations, Journal of Hydraulic Research, 49, 307–316, https://doi.org/10.1080/00221686.2011.566248, 2011.

Wang, Z., Walsh, K., and Verma, B.: On-Tree Mango Fruit Size Estimation Using RGB-D Images, Sensors, 17, 2738, https://doi.org/10.3390/s17122738, 2017.

Watkins, J., Tezaur, I., and Demeshko, I.: A Study on the Performance Portability of the Finite Element Assembly Process Within the Albany
955      Land Ice Solver, pp. 177–188, Springer International Publishing, Cham, https://doi.org/10.1007/978-3-030-30705-9_16, 2020.

Weill, S.: Modélisation des échanges surface/subsurface à l'échelle de la parcelle par une approche darcéenne multidomaine, Ph.D. thesis, Ecole des Mines de Paris, 2007.

Wittmann, R., Bungartz, H.-J., and Neumann, P.: High performance shallow water kernels for parallel overland flow simulations based on FullSWOF2D, Computers & Mathematics with Applications, 74, 110–125, https://doi.org/10.1016/j.camwa.2017.01.005, 2017.

960 Xia, J., Falconer, R. A., Lin, B., and Tan, G.: Numerical assessment of flood hazard risk to people and vehicles in flash floods, Environmental Modelling & Software, 26, 987–998, https://doi.org/10.1016/j.envsoft.2011.02.017, 2011.

Xia, X. and Liang, Q.: A new efficient implicit scheme for discretising the stiff friction terms in the shallow water equations, Advances in Water Resources, 117, 87 – 97, https://doi.org/https://doi.org/10.1016/j.advwatres.2018.05.004, 2018.

Xia, X., Liang, Q., Ming, X., and Hou, J.: An efficient and stable hydrodynamic model with novel source term discretization schemes for
965      overland flow and flood simulations, Water Resources Research, 53, 3730–3759, https://doi.org/10.1002/2016WR020055, 2017.

Xia, X., Liang, Q., and Ming, X.: A full-scale fluvial flood modelling framework based on a High-Performance Integrated hydrodynamic Modelling System (HiPIMS), Advances in Water Resources, p. 103392, https://doi.org/10.1016/j.advwatres.2019.103392, 2019.

Yu, C. and Duan, J.: Two-dimensional depth-averaged finite volume model for unsteady turbulent flow, Journal of Hydraulic Research, 50, 599–611, https://doi.org/10.1080/00221686.2012.730556, 2012.

970 Yu, C. and Duan, J.: Simulation of Surface Runoff Using Hydrodynamic Model, Journal of Hydrologic Engineering, 22, 04017 006, https://doi.org/10.1061/(asce)he.1943-5584.0001497, 2017.

Zhao, J., Özgen Xian, I., Liang, D., Wang, T., and Hinkelmann, R.: An improved multislope MUSCL scheme for solving shallow water equations on unstructured grids, Computers & Mathematics with Applications, 77, 576–596, https://doi.org/10.1016/j.camwa.2018.09.059, 2019.

Zhou, F., Chen, G., Huang, Y., Yang, J. Z., and Feng, H.: An adaptive moving finite volume scheme for modeling flood inundation over dry and complex topography, Water Resources Research, 49, 1914–1928, https://doi.org/10.1002/wrcr.20179, 2013.

## Appendix A: Additional validation test cases

This appendix contains an extended set of relevant test cases that are commonly used as validation cases in the literature. It complements and extends the verification evidence in section Section 4.

### A1 C-property: immersed bump

Using the same setup as in Section 4.1.1, but with a higher water surface elevation, in Figure A1 we demonstrate how SERGHEI-SWE conserves the C-property also for an immersed bump.
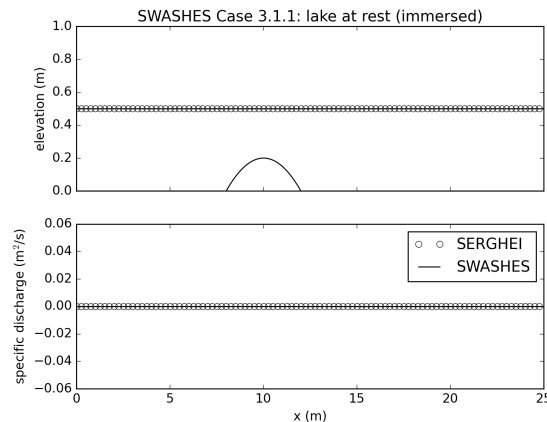


**Figure A1.** Lake-at-rest solution for an immersed bump

### A2 Well-balancing

To further show that SERGHEI-SWE is well-balanced, we computed three steady flows over a bump. We include a transcritical flow with a shock wave, a fully subcritical flow, and a transcritical flow , as shown in Figure A2. All of SERGHEI-SWE predictions show excellent agreement with the analytical solution. The constant unit discharge is captured with machine accuracy without oscillations at the shock, which is an inherent feature of the augmented Roe solver (Murillo and García-Navarro, 2010).

We also include two additional cases from MacDonald et al. (1995), for fully supercritical and subcritical flows in figure A3. These results and their L-norms in table **??** further confirm well-balancing.

Additionally, MacDonald-type solutions can be constructed for frictionless flumes to study the the bed slope source term implementation in isolation. We present a frictionless test case with SERGHEI-SWE that is not part of the SWASHES benchmark compilation. We discretise the bed elevation of the flume as

$$z(x) = C_0 - \frac{1}{2}\exp\left(-0.001x\right) - \frac{2q_0^2 \exp(0.002x)}{g}, \tag{A1}$$
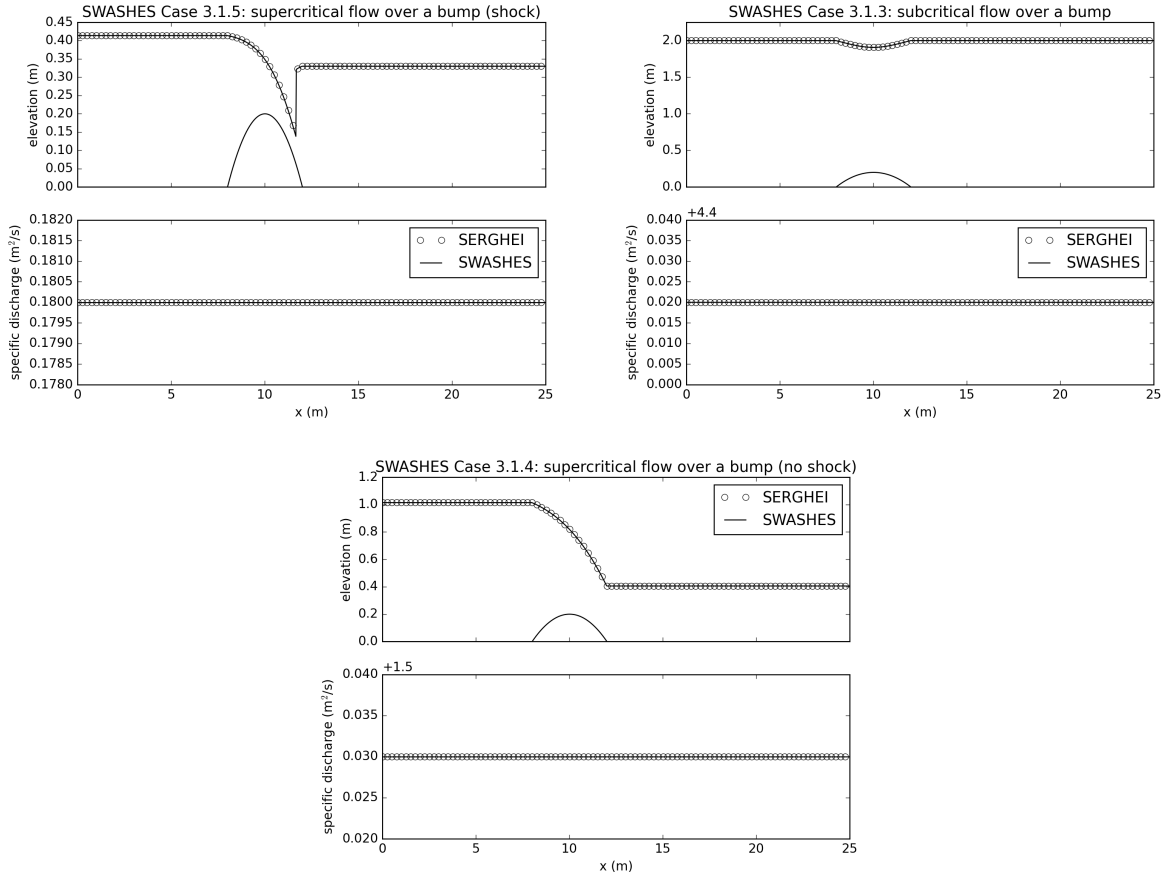
**Figure A2.** Analytical steady flows over a bump. SERGHEI-SWE captures moving equilibria solutions for transcritical flow with a shock (top left), fully subcritical flow (top right), and transcritical flow without a shock (bottom)

where $C_0$ is an arbitrary integration constant and $q_0$ is a specified unit discharge. The water depth for this topography is

$$h(x) = \frac{1}{2}\exp\left(-0.001x\right). \tag{A2}$$

Using $C_0 = 1.0$ m and $q_0 = 1.0$ m$^2$/s, we obtain the solution plotted in Figure A4. SERGHEI-SWE's prediction and the analytical solution show good agreement.

$L$-norms for errors in water depth are summarised in Table A1 for the sake of completeness. $L$-norms of a vector $\mathbf{x}$ with length $N$ and entries $x_i$, where $i \in [0, N) \subset \mathbb{Z}^+$ is the index of the entries, are calculated as

$$L_{\langle n \rangle} = \left(\sum_i^N |x_i|^{\langle n \rangle}\right)^{\frac{1}{\langle n \rangle}}, \tag{A3}$$
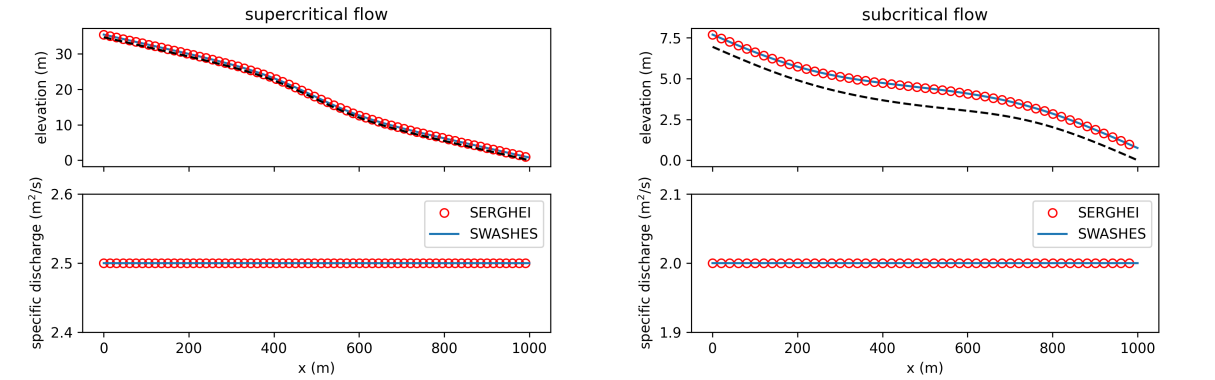
**Figure A3.** Analytical steady flows: Flumes. SERGHEI-SWE captures moving equilibria solutions for a subcritical (left) and supercritical (right) flow. Note that the solution is stable (no oscillations) and well-balanced (discharge remains constant along the flume).
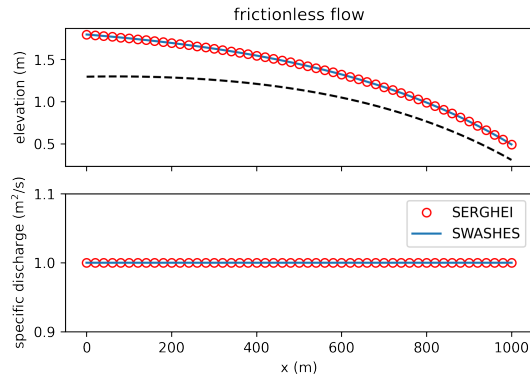


**Figure A4.** Analytical steady flows: Flumes. SERGHEI-SWE captures moving equilibrium solution for frictionless test case, with a stable and well-balanced solution.

with $\langle n \rangle \in \mathbb{Z}^+$ being the order of the $L$-norm. The $L_\infty$-norm is calculated as

$$L_\infty = \max |x_i|, \quad x_i \in \mathbf{x}. \tag{A4}$$

The $L$-norms for errors in unit discharge are in the range of machine accuracy for all cases and omitted here.

### A3 Dam break over a wet bed without friction

The dam break on wet bed without friction test case is configured by setting water depths in the domain as $h_L = 0.005\,\mathrm{m}$ and $h_R = 0.001\,\mathrm{m}$. The domain is $10\,\mathrm{m}$ long, and the discontinuity is located at $x_0 = 5\,\mathrm{m}$. The total run time is $6\,\mathrm{s}$. Figure A5 shows the model results obtained on successively refined grids, compared against the analytical solution by (Stoker, 1957). Errors for this test case are reported in Table A2. We also report the observed convergence rate $R$, calculated on the basis of the

| Case | $L_1$ (m) | $L_2$ (m) | $L_\infty$ (m) |
|---|---|---|---|
| Figure A1 | 0.0 | 0.0 | 0.0 |
| Figure A2(top left) | 0.371 | 0.07285 | 0.06984 |
| Figure A2(top right) | 0.293 | 0.02618 | 0.00332 |
| Figure A2(bottom) | 0.693 | 0.0306 | 0.00356 |
| Figure A3(left) | 5.21459 | 0.12162 | 0.00435 |
| Figure A3(right) | 1.0389 | 0.03805 | 0.00191 |
| Figure A4 | 0.74571 | 0.02743 | 0.00178 |

**Table A1.** Analytical steady flows: Summary of $L$-norms for errors in water depth; $L$-norms for errors in unit discharge are in the range of machine accuracy and omitted here.
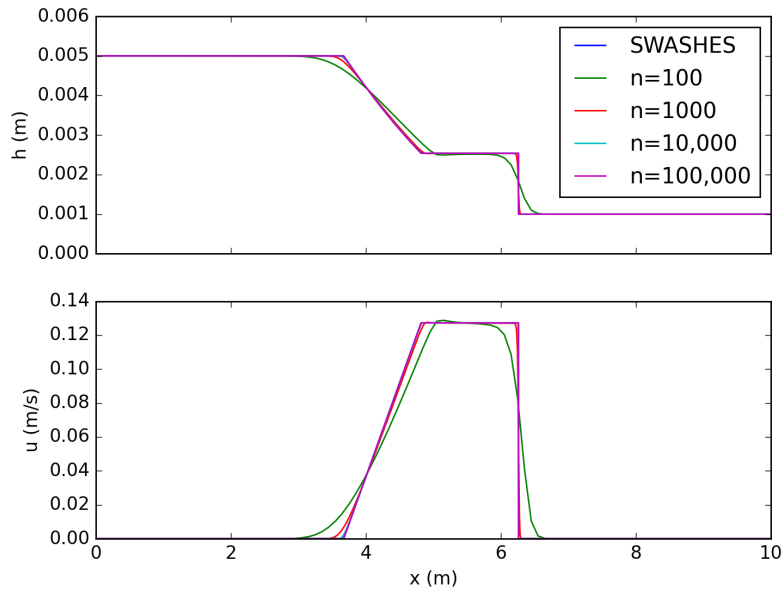


**Figure A5.** Dam break on wet bed without friction: Model predictions for different number of grid cells. SERGHEI-SWE converges to the analytical solution (Stoker's solution) as the grid is refined.

$L1$-norm. As the grid is refined, the model result converges to the analytical solution. Due to the discontinuities in the solution, the observed convergence rate is below the theoretical convergence rate of $R = 1$.

| n | L1(h) (m) | L2(h) (m) | R(h) (m) | L1(u) (m/s) | L2(u) (m/s) | R(u) (m/s) |
|---|---|---|---|---|---|---|
| 100 | 0.01623 | 0.03303 | - | 0.11194 | 0.14115 | - |
| 1000 | 0.00265 | 0.00932 | 0.79 | 0.01842 | 0.0424 | 0.78 |
| 10000 | 0.00041 | 0.00327 | 0.81 | 0.00272 | 0.01458 | 0.83 |
| 100000 | $6 \times 10^{-5}$ | 0.00125 | 0.83 | 0.00037 | 0.00581 | 0.87 |

**Table A2.** Analytical dam break: L-norms and empirical convergence rates (R) for water depth ($h$) and velocity ($u$)

## A4 Radially-symmetrical paraboloid

Using the same computational domain and bed topography as the case in Section 4.3, results for the radially symmetrical oscillation in a frictionless paraboloid (Thacker, 1981) are presented here. The details about the initial condition and the analytical solution for the water depth and velocities can be found in (Delestre et al., 2013). Particularly, the analytical solution at $t = 0\,\text{s}$ is set as initial condition and three periods are simulated using $\delta x = 0.01\,\text{m}$ as the grid resolution. Figure A6 shows the numerical and analytical solution at four different times. Although the analytical solution is periodic without dumping, the numerical results show a diffusive behaviour attributed to the numerical diffusion introduced by the first order scheme. Other than that, model results show good agreement with the analytical solution.

## A5 Experimental laboratory scale tsunami

A 1:400 scale experiment of a tsunami run-up over the Monai valley (Japan) was reported by (Matsuyama and Tanaka, 2001; The third international workshop on long-wave runup models, 2004), providing experimental data on the temporal evolution of the water surface at three locations, and of the maximum run-up. A laboratory basin of $2.05 \times 3.4\,\text{m}$ was used to create a physical scale model of the Monai coastline. A tsunami was simulated by appropriate forcing of the boundary conditions. This experiment has been extensively used to benchmark SWE solvers (Arpaia and Ricchiuto, 2018; Caviedes-Voullième et al., 2020b; Hou et al., 2015, 2018; Kesserwani and Liang, 2012; Kesserwani and Sharifian, 2020; Morales-Hernández et al., 2014; Murillo et al., 2009; Murillo and García-Navarro, 2012; Nikolos and Delis, 2009; Serrano-Pacheco et al., 2009; Vater et al., 2019). The domain was discretised with a resolution of $1.4\,\text{cm}$, producing 95892 elements. Simulated water surface elevations are shown together with the experimental measurements in Figure A7 at three gauge locations. The results agree well with experimental measurements, both in the water surface elevations and the arrival times of the waves.

## A6 Experimental dam-break over a triangular sill

Hiver (2000) presented a large flume experiment of a dam-break over a triangular sill, which is a standard benchmark in dam-break problems (Caviedes-Voullième and Kesserwani, 2015; Bruwier et al., 2016; Kesserwani and Liang, 2010; Loukili and Soulaïmani, 2007; Murillo and García-Navarro, 2012; Yu and Duan, 2017; Zhou et al., 2013), together with the reduced scale version (Soares-Frazão, 2007; Hou et al., 2013a, b; Yu and Duan, 2017).
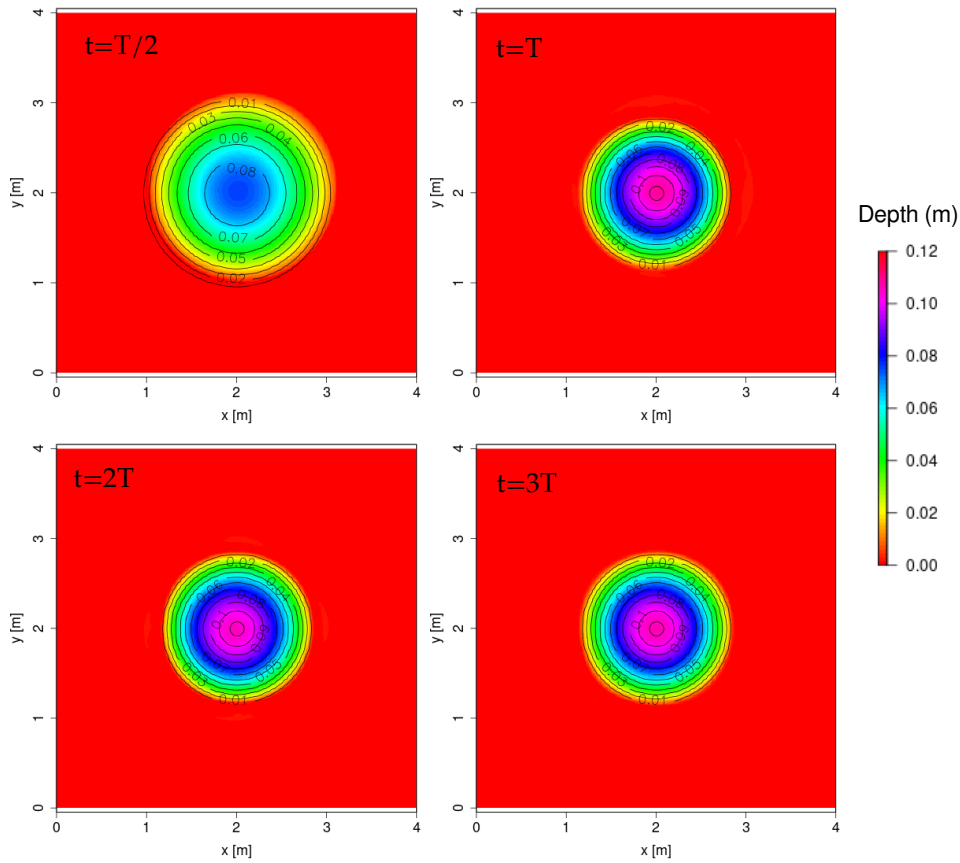
**Figure A6.** Radially-symmetrical paraboloid: Snapshots of water depth by the model compared to the analytical solution (contour lines). Period $T = 2.242851\,\text{s}$
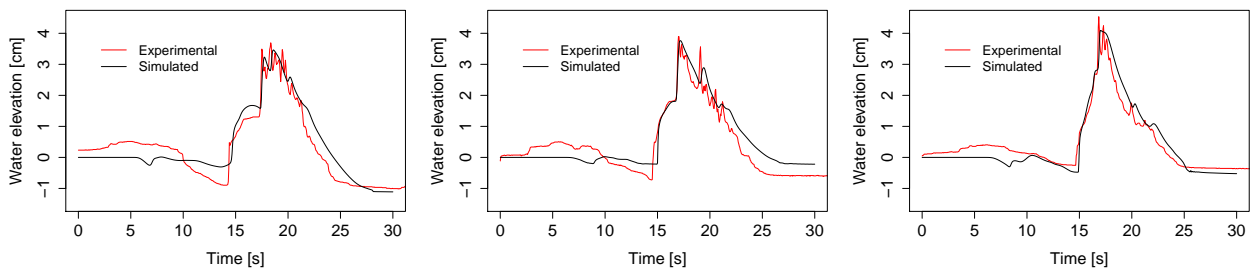


**Figure A7.** Simulated and experimental results for the laboratory scale tsunami case at gauges G1 (left), G2 (centre) and G3 (right).

The computational domain was discretised with a $380 \times 5$ grid, with a $\delta x = 0.1\,\text{m}$ resolution. Figure A8 shows simulated and experimental results for the triangular sill case. A very good agreement can be observed, both in terms of peak depths

46

occurring whenever the shock wave passes through a gauge, and in the timing of the shock wave movement. The simulations tend to slightly overestimate the peaks of the shock wave, as well as overestimating the waves downstream of the sill (see plot for gauge at $x = 35.5\,\text{m}$). Both behaviours are well documented in the literature.
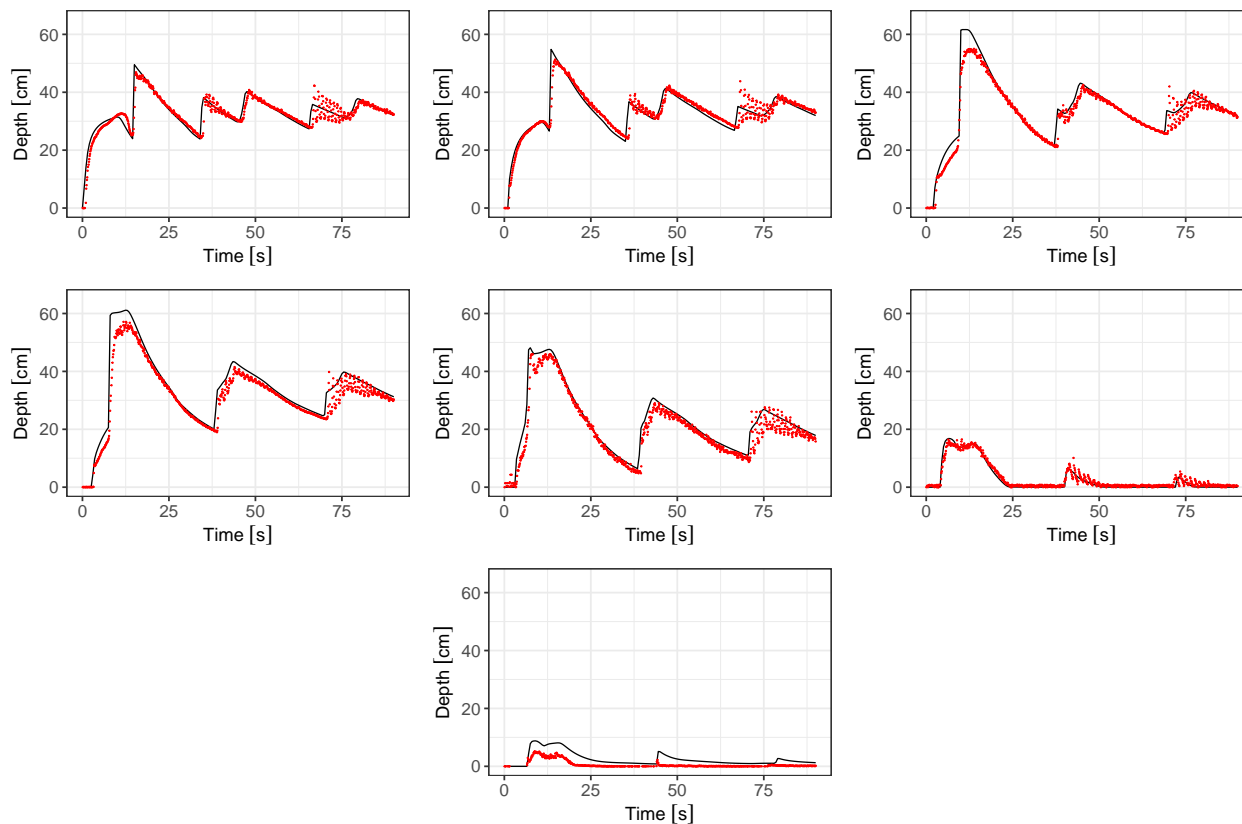


**Figure A8.** Simulated (black lines) and experimental (red points) transient water depths at seven gauge points ($x = 17.5$, $x = 19.5$, $x = 23.5$, $x = 25.5$, $x = 26.5$, $x = 28.5$, $x = 35.5$, from top left to bottom right) for the the dam-break over a triangular sill.

## A7 Experimental idealised urban dam-break

A laboratory-scale experiment of a dam-break over an idealised urban area was reported by (Soares-Frazão and Zech, 2008) in a concrete channel including 25 obstacles representing buildings separated by $10\,\text{cm}$. It is widely used in the shallow-water community (Abderrezzak et al., 2008; Caviedes-Voullième et al., 2020b; Ginting, 2019; Hartanto et al., 2011; Jeong et al., 2012; Özgen et al., 2015a; Petaccia et al., 2010; Wang et al., 2017) because of its fundamental phenomenological interest and because it is demanding in terms of numerical stability and model performance. The small buildings and streets in the geometry require sufficiently high resolution , both to capture the geometry, and to capture the complex flow phenomena which is triggered in the streets. Experimental measurements of transient water depth exist at different locations, including in

between the buildings. A resolution of $2\,\mathrm{cm}$ was used for the simulated results in Figure A9, together with experimental data. The results agree well with the experimental observations, to a similar degree as what has been reported in the literature.
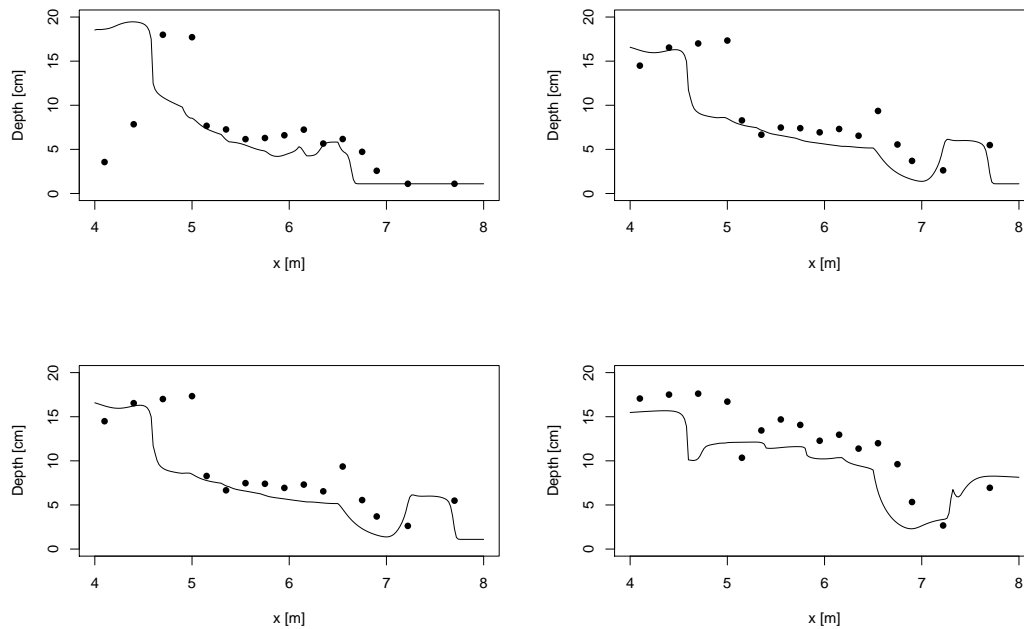


**Figure A9.** Simulated (lines) and experimental (points) water depth profiles at $y = 0.2\,\mathrm{m}$, at four times (4, 5, 6 and 10s, top left to bottom right), for the idealised urban dam-break case.

## 1050 A8 Experimental rainfall-runoff over a dense idealised urban area

Cea et al. (2010b) presented a laboratory scale experiment in a flume with a dense idealised urban area. The case elaborates on the setup of Cea et al. (2010a) (Section 5.3), including 180 buildings (case L180), in contrast to the 12 buildings in Section 5.3, which potentially requires a higher resolution to resolve the building (6.2 cm sides) and street width ($\sim 2\,\mathrm{cm}$), and the flow in the streets. We keep a 1 cm resolution. Rainfall is a single pulse of constant intensity. Two setups were used with intensities 1055 $180\,\mathrm{mm\,h^{-1}}$ and $300\,\mathrm{mm\,h^{-1}}$ and duration of 60s and 20s respectively. As Figure A10 shows, the hydrographs are well captured by the simulation, albeit with a delay. Analogously to Section 5.3, this can be attributed to surface tension in the early wetting phase.
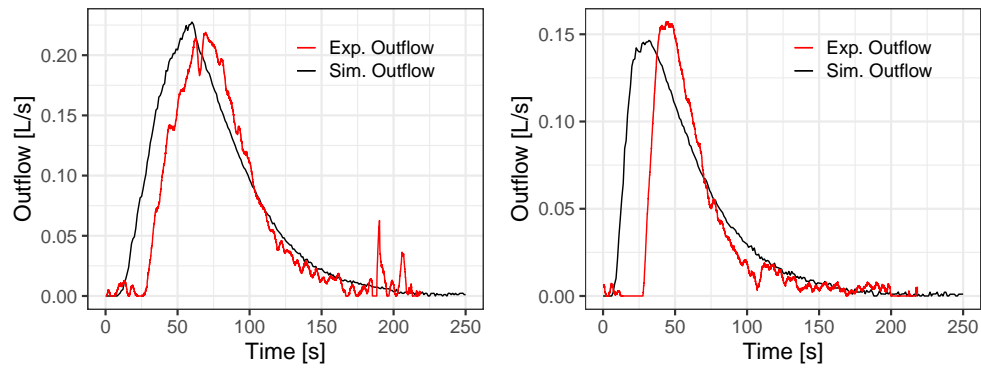
**Figure A10.** Simulated hydrographs compared to experimental data from Cea et al. (2010b) for two rainfall pulses on the L180 building arrangement. Left: rainfall intensity $180\,\mathrm{mmh^{-1}}$, duration $60\,\mathrm{s}$. Right: rainfall intensity $300\,\mathrm{mmh^{-1}}$, duration $20\,\mathrm{s}$